

Detection and visualisation of terrain edges in slope failures

Martina Slámová ^{a*} , Roman Sitko ^b , Roman Kadlečík ^b,
Ľuboš Skurčák ^c , František Chudý ^b

Abstract

Our aim was to develop a pixel-based methodology employing multiple terrain parameters for the semi-automatic identification of terrain edges. The procedure was applied to landform features associated with slope failures, operating on different resolutions of a digital terrain model (DTM). We intended to produce two outputs – grid maps based on: discrete data allowing precise identification and revealing a higher incidence of terrain edges than a hillshade map; floating point data visually highlighting terrain edges more sharply than a hillshade grid. The results showed that the grid maps generated by the new method: Binary Terrain Edges – BinT and Quality Terrain – QT exhibited more terrain edges than the hillshade map. The method demonstrated its robustness when used across three different resolutions of DTM. It was applied within the protection buffer zone of the overhead transmission powerline (OHL). Slightly more than half of the total of identified and manually digitised slope failures using the hillshade map supplemented with failures observed in QT may not necessarily be subject to field confirmation. OHL is a long-distance construction passing a variety of environments. Therefore, the detection of slope failures requires semi-automatic or automatic procedures to be costless and time-saving.

Keywords: Terrain edges, binary grid, quality terrain, pixel-based methods, digital terrain model, LiDAR

Article history: Received 13 February 2024, Accepted 26 March 2025, Published 30 June 2025

1. Introduction

Slope failures have serious consequences for land cover and constructions (Aigbadon et al., 2021). A landslide hazard map or model produced using GIS technologies is usually a common tool used to mitigate or prevent slope movement (Liu et al., 2021). Verification of slope failures identified in digital products is routinely carried out in the field by geological experts, often in collaboration with geodesists (Prokešová et al., 2010; Podolszki et al., 2022). Today's technology makes it possible to accurately identify slope failures, even subtle ones, in detailed and accurate digital terrain models (DTMs) where field verification would not be necessary (Ortuño et al., 2017). The advantage of using hillshaded derivatives of DTMs is the visual highlighting of landforms that are difficult or impossible to identify from aerial photographs or field observations (Van Den Eeckhaut et al., 2007). However, many researchers still recommend selective field validation to improve the reliability of landslide mapping outputs, particularly when the datasets or the algorithms involved are untested in specific geological or environmental settings (Jaboyedoff et al., 2018).

Geohazards intersecting with technical and urban constructions may result in significant economic damages (Liščák et al., 2010). The Slovak republic has no national report accounting slope failures within urban structures or energy infrastructure. Strategies for landslide prevention are outlined in the "Program for the Prevention and Management of Landslide Risks (2014–2020)" (Ministry of the Environment of the Slovak Republic, 2018). An

engineering geological survey conducted between 2018–2019 identified 13 sites with the most severe landslides, demanding considerable attention due to their associated risk to life and properties (Mašlár et al., 2020). Semi-automatic detection of landslides would accelerate the updating of current databases.

The research presented in the article deals with one of the project's objectives that was carried out in cooperation with the Nuclear Power Plant Research Institute (VUJE a.s.). The project purpose was to produce two outputs that would be useful for overhead power line (OHL) maintenance: 1) a method for classifying tree species – a model for predicting their growth under the power line; 2) a method for semi-automatic identification of terrain edges indicating the presence of slope failures. An area under investigation was a protection buffer zone of 100 m to each side from the transmission powerline. In the Carpathian Mountains of the Slovak Republic, OHLs are often located in steep and rugged terrain, usually covered by forests. This is also the case in this study. Therefore, the identification of slope failures requires specific procedures to make mapping efficient – fast and costless.

2. Theoretical background

2.1 Identification of slope failures features in high-resolution digital terrain models

A classification by Cruden & Varnes (1996) updated by the British Geological Survey (2024) defines the basic types of landslides: falls,

^a UNESCO Department for Ecological Awareness and Sustainable Development, Faculty of Ecology and Environmental Sciences, Technical University in Zvolen, Slovakia (corresponding author: M. Slámová, e-mail: martina.slamova@tuzvo.sk)

^b Department of Forest Resource Planning and Informatics, Faculty of Forestry, Technical University in Zvolen, Slovakia

^c VUJE, a. s., workplace Košice, Department of Science, Research, Development and Analysis, Košice, Slovakia

topples, slides (rotational and translational) and flows. Landslides are characterised by the following features: crown, main scarp, top, head, minor scarp, main body, foot, tip, toe, surface of rupture, toe of surface of rupture, surface of separation, displaced material, zone of depletion, zone of accumulation, depletion, depleted mass, accumulation, flank, and original ground surface. A spatial model (Fig. 1a) shows the features – subtle landforms examined in this study and the features of the real landslide, one of several, which were identified in the study area (Fig. 1b). Although they span a few decimetres or metres, they play a crucial role in identifying an initial phase of slope movement.

Subtle landforms can be identified within high-resolution airborne Light Detection and Ranging (LiDAR) DTMs (Abellan et al., 2016; Mora et al., 2018; Chudý et al., 2018a,b; Martins et al., 2020). The main limitation lies in the point density of the LiDAR dataset (Pirotti & Tarolli, 2010). High-resolution DTMs enable the measurements of multi-temporal slope displacements (Fernández et al., 2017). The Unmanned Aerial Vehicle (UAV) is a relatively low-cost technology for obtaining detailed aerial images. The applicability of UAV data depends on the Structure-from-Motion (SfM) software processing of the photogrammetric material and the drone pilot's ability to navigate the UAV over the slope failure in complex natural settings (Giordan et al., 2020). It allows regular surveys to produce a time series of high-resolution images (Rossi et al., 2018; Mercuri et al., 2023). Even, Digital Surface Models (DSMs) which are produced in detail and high accuracy allow a series of measurements of slope failures variables to compute volumetric changes (Turner et al., 2015; Du et al., 2023). The most detailed mapping and assessment of spatio-temporal morphological change in any area is provided by combining data from geomorphological field surveys, LiDAR and UAVs (Borrelli et al., 2019). However, applying this approach on a wide scale is technologically demanding and takes a long time to process heavy datasets.

Landforms such as gullies, dunes, lava fields and landslides, all have similar features exhibiting high roughness contrast to the surrounding terrain. Thus, terrain roughness is an important variable to capture these features in DTMs (Korzeniowska et al., 2018). It is formed by sharply curved terrain edges. They are defined as significant local changes which are found on the border between two different regions. Edge detection is considered to be an initial step in the process of retrieving information from an image (Cesar & Costa, 1995). Edge detection techniques are generally divided into object-oriented and pixel-based methods, combination of both methods (Li & Wan, 2015; Zhao et al., 2017; Syzdykbayev et al., 2020) and spatial data mining methods (Hussain et al., 2013). Pixel-based and object-based classification methods differ in two aspects: classification units and classification features (Liu & Xia, 2010).

While a number of studies have demonstrated the advantages of object-based classification over pixel-based classification (Liu & Xia, 2010), less attention has been paid to the potential limitations of the image segmentation algorithm (Kampouraki et al., 2008). A main restriction of the pixel-based analysis is a lack of correspondence between landslide size and pixel size (Domènech et al., 2019). However, it can be overcome with additional data from LiDAR with a very high resolution (Chudý et al., 2019). Although pixel-based methods do not work with real objects, their advantage is the availability of a wide range of statistical operators in any GIS application (Hussain et al., 2013). This was a factor in the decision to use a pixel-based algorithm in this research.

2.2 Semi-automatic methods to identify terrain edges

Classifying landslide patterns from DTMs has been the subject of numerous studies (Razak et al. 2011; Al-Rawabdeh et al., 2016; Mărgărint & Niculiță, 2017; Masruroh et al., 2023). Slope failures are usually manually digitised based on their visual interpretation from aerial photographs and subsequently confirmed by field surveys (Długosz, 2012). A hillshade map is commonly used to identify and delineate slope failures (Van Den Eeckhaut et al., 2005). However, it has not been proven to be sufficiently effective in identifying subtle landforms that do not cast enough strong shadows (Jagodnik et al., 2020; Jagodnik, 2024).

Current literature lacks approaches on semi-automatic classification specifically addressing subtle landforms of slope failures (Jagodnik, 2024). This procedure demands firstly, very precise DTM and secondly, a combination of diverse tools to extract these features from digital models (Mayoral et al., 2017; Lee et al., 2017; Lieskovský et al., 2022). Interpretation of the slope failures features facilitates the identification of their patterns. It is an essential input for machine learning algorithm or the development of spatial landslide models based on topographic zoning (Masruroh et al., 2023). Extraction of these features can be performed in eCognition Developer, a software development kit that uses an object-oriented approach to semi-automated image analysis (Shruthi et al., 2011). The authors noted that the accuracy uncertainty of the classified objects needs to be revalidated or corrected by other methods, and that the results also contain false positives. However, it should be noted that other methods may also produce false positives. Another popular method for detecting landform patterns in DTM is Geomorphon. It is a geomorphon tool that operates under Geographic Resources Analysis Support System (GRASS) GIS and Quantum (QGIS) GIS applications. The algorithm allows to recognise common local morphological elements such as flats, peaks, ridges, shoulders, spurs, slopes, hollows, footslopes, valleys, and pits (Jasiewicz & Stepinski, 2013). However, it is not designed to detect the subtle

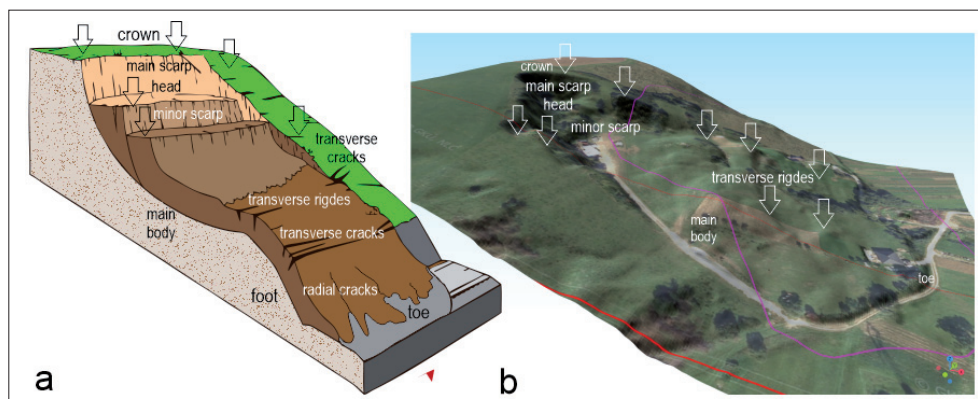


Fig. 1: A general model of a slope failure (a), a real landslide demonstrating the features investigated in this study (b)
Source: Author's conceptualisation (a), The Geodesy, Cartography and Cadastre Authority of the Slovak Republic: DMR5.0 (1 m)-JTSK(JTSK03) and ortho-photomosaic, State Geological Institute of Dionýz Štúr: slope failures; modified by the author (b)

landforms of terrain edges on slopes. A method that was primarily, but not only, designed to detect subtle landforms developed Zhou et al. (2018). These performed multi-neighbourhood analysis to determine the edges of linear terrain features of ridge, shoulder, valley and foot-slope and defined a probabilistic visual descriptor for quantifying edge pixels. The technique of edge detection usually begins with the filtering to reduce data noise, followed by enhancement to identify changes in the intensity between two different regions and finishes with the detection of lines with strong edge content (Cesar & Costa, 1995). These methodological steps sketched a concept for a newly proposed method.

2.3 The aim

The aim of the article was to develop a methodology for semi-automatic identification of pixels interpreting sharply curved terrain edges of scarps, cracks and transverse ridges in the main landslide's body and its accumulation zone (Fig. 1a,b). We intended to develop an algorithm to detect pixels with “strong edge content”, as defined by Cesar & Costa (1995), instead of lines, which are interpreted as vectors and are the output of the object-oriented methods. Terrain edges detected by the new method would contrast sharply with the smooth slopes around them.

A new method is designed to work with digital formats of a grid map based on:

- Discrete data allowing precise identification and revealing terrain edges of subtle landforms, and the main output is binary grid of terrain edges (Binary Terrain Edges, BinTerrain, BinTE);
- Floating-point data visually highlighting terrain edges, and the main output is grey-shaded grid of terrain edges (Quality Terrain, QTerrain, QT).

In terms of the method applicability, we assume that:

- Both grid maps produced by the new method exhibit more terrain edges than could be detected in the hillshade map;
- It could be applied on DTMs with different resolutions, allowing objects to be studied at different scales;
- The usability of the grid map on steep slopes above 25° may be limited due to the low contrast between the terrain edges of slope failures and other landforms in their vicinity.

3. Data and methods

3.1 Study area

The wider area of slope failures alongside the OHL under investigation is located in the north-western part of the Slovak Republic near the towns of Považská Bystrica and Žilina and covers an area of 10,897 hectares. The terrain edge survey was

carried out within the OHL buffer zone, which is 100 metres on either side of the transmission line, with a total length of 55 kilometres and an area of 1,090 hectares (Appendix 1). The geological environment is an important indicator of potential slope failures and they were identified on a public 1:50,000 scale map (Šimeková et al., 2006) within the wider study area (Fig. 2, black line). Their coverage was evaluated using QGIS application. Slope failures occurred over 470 ha (4%) of the wider area. Of these landslides, 28 ha were active, 226 ha potential, and 216 ha were stabilised forms. The Quaternary Geological Map of the Slovak Republic (Maglay et al., 2011) indicated two landslides (Fig. 2, red line). The presence of slope failures was the main criterion for the selection of study sites and the production of a high resolution DTM used for terrain analysis.

The proposed method was applied to three sites, designated A, B and C, and located in different geological formations and natural environments (Tab. 1). Sites A and B are landslides and they were chosen to demonstrate the efficiency of the method on different slopes. Site C demonstrates the applicability of the method on different DTM resolutions. Extra dense LiDAR data were not available for sites A and B. Therefore, site C was considered for the investigation. It is U-shaped gully with minor scarps on its banks and exposed bare substrate in its upper parts. This is the case of the morphological structure that could pose a potential risk for the development of deep-seated slope slides. Although this is not the case at the study site, as noted by the authors (Parkner et al., 2007), it is important to identify and monitor gullies in certain landslide-prone areas. Since site C is not the landslide, the results are presented in the appendix.

3.2 Data acquisition

The maps used in the research were obtained from public repositories. Digital terrain models were generated from DMR3.5 and DMR5.0 datasets which are freely available at public portals (The Geodesy, Cartography and Cadastre Authority of the Slovak Republic, 2023a, b, c). DMR5.0 is a product of high-resolution LiDAR with a point cloud density of 5 points/pixel with overall vertical accuracy equal to or less than 0.25 metres, and horizontal accuracy equal to or less than 0.50 metres (The Geodesy, Cartography and Cadastre Authority of the Slovak Republic, 2023c). DMR5.0 covers the full length of the OHL construction. DMR5.0 with a resolution of 1 metre per pixel was used in pivotal results detailing the subtle landforms of slope failures. The declared resolution of DMR5.0 is considered sufficient to detect terrain edges, as confirmed by other studies (Azizi et al., 2014; Ortuño et al., 2017).

Further, an extra dense LiDAR point clouds were provided by VUJE a.s. and captured were from a helicopter using the RIEGL VP-1 LiDAR scanner and acquired in the period between April

Site	A	B	C
Geomorphological units ^(a)	Rajecká Kotlina Basin, a subunit of Žilinská Kotlina Basin	Lučanská Malá Fatra Mts., a subunit of Malá Fatra Mts.	Podmanínska Pahorkatina Upland, a subunit of Považské Podolie Valley
Regional geology ^(a)	Inner Carpathian Palaeogene	Core Mountain Range	Klippen Belt Mountain Range (Puchov section)
Bedrock ^(a)	Deluvial-polygenetic sediments: clayey-clayey and sandy slope clays	Gutenstein beds – Gutenstein (Annaberian) limestones: dark grey and black coarse-grain, layered, worm-like limestones; Ramsar dolomites: grey layered dolomites	Sandstones, silts, calcareous claystones, laminated silts and sills, and conglomerates
Climate-geographic type ^(a)	Basin climate, slightly cool	Mountainous climate, cold	Mountainous climate, moderately warm
Annual rainfall interval [mm] ^(a)	600–850	800–1100	600–850
Annual air temperature (1961–1990) average [°C] ^(a)	7.5	6.5	7.5
Slope mean ^(b)	9°	18°	9°

Tab. 1: Geomorphology, geology and climate of the study sites

Sources: (a) State Geological Institute of Dionýz Štúr: geomorphology, geology and bedrock, climate, rainfall and temperature, (b) The Geodesy, Cartography and Cadastre Authority of the Slovak Republic – DMR5.0 (1 m) JTSK(JTSK03): slope, modified by the author

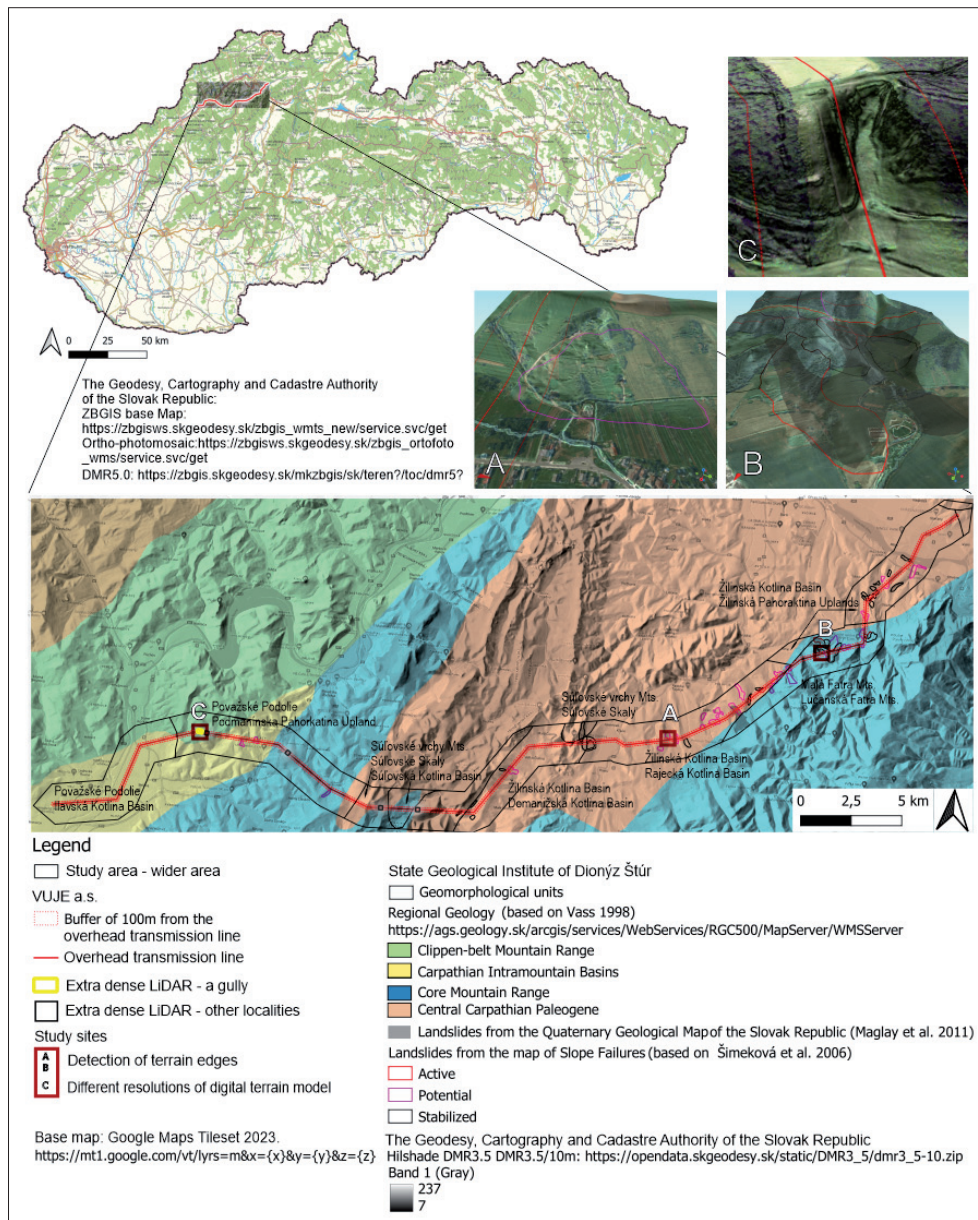


Fig. 2: The study area in the Slovak Republic and sites A, B and C

Source: VUJE a.s.: overhead transmission powerline, poles and protection zone, State Geological Institute of Dionýz Štúr: slope failures, regional geology and geology, The Geodesy, Cartography and Cadastre Authority of the Slovak Republic: Hillshade DMR3.5, Google Maps Tileset, modified by the author

and June 2023. RIEGL VP-1 had minimum scanning range of 5 m, accuracy 15 mm, precision 10 mm, maximum effective measurement up to $750,000 \text{ meas.s}^{-1}$ (820 kHz PRR & 330° FOV), laser pulse repetition mode up to 820 kHz, near infrared laser wavelength, echo signal density for each echo signal high resolution, laser beam divergence 0.5 mrad. A point density varied from 484 PPSM (points per square metre) for all returns to 254 PPSM for the last returns to assess the applicability of the proposed method at sub-metre resolution. The LAS files were converted to the LAZ format, following the procedure published by Chudý et al. (2019). LAStools application was used to isolate ground return points. These points were converted to the vector format, and a fine-scale DTM was created using the TIN interpolation module in geographic information system (GIS) application. Using the original quarter mm (0.00025 metre) resolution of the LAS x,y,z tuples, a very high resolution DTM was produced at 0.15 metres per pixel. The original LAS format was projected in the S-JTSK [JTSK03] / Krovak East North (EPSG:8353) coordinate system.

VUJE a.s., provided also information about the OHL construction, its buffer zone of protection (100 m) and poles of the high voltage power line.

The datasets were processed using QGIS 3.28.10-Firenze, licensed under the GNU General Public License, and LAStools-a LiDAR processing software (version 220613, unlicensed). Spatial visualisations of subtle landforms were processed using the QGIS2threejs exporter plugin (QGIS Python Plugins Repository, 2022) and the EPSG 5514 coordinate system was set-up to process and render outputs.

3.3 Manual digitisation of slope failures in a hillshade map

Manual delineation of slope failures using a hillshaded map is a conventional technique applied in many recent studies (Van Den Eeckhaut et al., 2005; Długosz, 2012). We digitised slope failures in locations where we could visually detect terrain edges of subtle landforms indicating slope failures. Number and area [ha] were evaluated using the Field Calculator in QGIS.

3.4 New method – morphometric variables used to identify terrain edge

Local primary morphometric variables allow the detection of subtle landforms. They are calculated based on their immediate surroundings, derived directly from the DTM without additional input, and can be calculated independently of the wider area represented.

Slope is one such variable. It is a derivative of altitude (first derivation), measuring the maximum change in elevation relative to the distance between a cell and its eight neighbours (Barbosa et al., 2021). The slope gradient plays a pivotal role in movement tendencies. Slopes prone to landslides are expected to be predominantly between 30° and 45° (Guthrie & Evans, 2004) or between 15° and 25°, while those above 25° commonly experience shallow slides (Zežere, 2002; Frattini et al., 2004). In the detection of landslide topography, slope is commonly fused with other elevation derivatives (Berti et al., 2013; Mora et al., 2018).

Terrain roughness, an efficient way to differentiate various landforms, displays elevation variability within a defined radius but it is highly sensitive to scale (Schillaci et al., 2015). Maximum curvature of the terrain was computed, rather than the terrain roughness, for the purposes of this research. Curvature is a second derivation of altitude. It highlights the convexity or concavity of the terrain. Positive values indicate convex, negative concave and zero values indicate planar landforms on slopes (Evans & Cox, 1999; Shary et al., 2002; Wilson, 2012). Local directions of maximum curvatures indicate the steepest variation of the surface normal (Alliez & Desbrun, 2002). Maximum curvature is an attribute that is very powerful in delineating defects and defect geometries (Roberts, 2001). The SAGA module of Terrain Analysis – Morphometry: Slope, Aspect, Curvature module was used to calculate maximum curvature and slope (SAGA-GIS Tool Library Documentation, 2001).

Sky view factor is a solar variable that is the secondary morphometric variable calculated to quantify interactions between the Earth's surface and the atmosphere (Wilson, 2012). These variables, interpreted in raster formats as shaded terrain, emphasise the brightness and contrast of landform discontinuities. The sky view factor visualises micro-landforms regardless of their orientation to the cardinal points. Diffuse light overcomes directional problems associated with hill shading (Kokalj & Somrak, 2019), and when combined with slope parameters, shaded terrains exhibit distinct terrain edges (Mayoral et al., 2017). In this study, we applied the sky view factor (SAGA-GIS Module Library Documentation v2.2.0, 2008), which ranges from 1 for completely unobstructed surfaces to 0 for completely obstructed surfaces (Harris & Baird, 2018). The search radius was set to 100 metres for the LiDAR DMR3.5 and 5.0, and 5 metres for the extra dense LiDAR data.

3.5 New method – calculation of terrain edge

3.5.1 A grid map based on discrete data

While the proposed method is pixel based, then terrain edges were evaluated in a grid form as pixels and not as vector lines. To identify the discontinuities in the terrain, the raster calculator was employed in operations on raster to multiply the slope and sky view factor grid layers. Maximum curvature values were displayed using a discrete colour ramp and interpreted within quantile ranges, typically used for ordinal data ranking within categories (GISGeography, 2023). Thresholding is common procedure in terrain analysis and its output is a binary classification in which data values above certain thresholds can be identified as target features (Zhou et al., 2018). Thus, values of the class representing the most convex landforms (higher than 0.0496 in this study) were used to compute a binary grid “BinaryMaximumCurvature”. Further, the binary grid was subtracted from the “Slope” grid,

multiplied by “SkyViewFactor” and saved as “TerrainEdges”. This mathematical operation simply removes repetitive, and therefore redundant pixels (ARCGISpro, 2023).

A pseudo formula of the calculation follows:

$$\begin{aligned} \text{OutputRaster}(\text{“TerrainEdges”}) &= \\ &= \text{Raster}(\text{“Slope”} * \text{“SkyViewFactor”}) - \text{Raster}(\text{“BinaryMaximalCurvature”}) \end{aligned}$$

The output of “TerrainEdges” was again interpreted with discrete symbology using quantile distribution values. Then it was reclassified to a binary grid using a threshold of the class with the highest values (higher than 0.0310 in this study) representing terrain edges. The output was saved as “BIN_TERRAIN_EDGES” (BinTE). This is the first product of the proposed methodology. A visual comparison reveals a clear distinction between the “BinaryMaximalCurvature” and “BIN_TERRAIN_EDGES” grids. BinTE contains less pixels but matches better terrain edges (Fig. 3).

3.5.2 A grid map based on floating-point data

To create a training dataset for the supervised classification in the next step, a raster was converted to a vector format of an ESRI shapefile using the Polygonise function. Further adjustments were made to remove redundant data, which means areas smaller than 4 m², consisting of three adjacent pixels in each direction. A vector output of “BIN_Terrain_Edges_4px” was created. In the extra dense LiDAR dataset, polygons with an area of 0.0225 m² were removed. Polygons derived from the DMR3.5 derivative were not adjusted due to the relatively small study area (a slope failure in study area C was up to 4 ha), which did not allow the removal of any pixels from the 10m/px DTM to maintain output accuracy. The main purpose of this step was to create a training vector dataset that best fits the target shapes of a pattern of terrain edges specific to the landforms being investigated. However, if it is necessary to preserve detailed terrain edges for any research purposes, this pixel removal step can be omitted.

SAGA Supervised Classification module (SAGA-GIS Tool Library Documentation v2.2.0, 2005) was employed to generate a “QUALITY_TERRAIN”(QT) – a floating-point raster that simulates shaded terrain and visually emphasises sharp, convex terrain edges indicating slope failures. QT is the second output of the proposed methodology. The process of the SAGA Supervised Classification involved a grid of “Slope” multiplied by “SkyViewFactor”. Statistics were loaded from “BinaryMaximumCurvature”. The training class was set up as a single value column, representing a specific target shape to be highlighted as the main output of the grey shaded grid. Chosen was the minimum distance method with the probabilistic reference set to relative. The default thresholds for distance, angle and probability were maintained default. The intricate shapes of the polygons “BIN_Terrain_Edges_4px” derived from three different sites (A, B, and C), are anticipated to exert an influence on each single result of the supervised classification of “QUALITY_TERRAIN”.

The Supervised Classification is primarily a tool designed to categorise land cover based on spectral imagery, using training sites of known land cover and user-defined land cover. It classifies pixels by grouping them into classes according to the spectral data of the training site pixels (SAGA-GIS Tool Library Documentation v2.2.0, 2005). The intended usage for this research was different. We did not expect to produce an exact classification. We anticipated to get a range of values which could be divided into two groups. One group indicated a high level of confidence and reliability in the final output grid, while the other, with values close to zero, indicated a high level of uncertainty. Cesar & Costa (1995) defined edges as significant local changes at the border of different region.

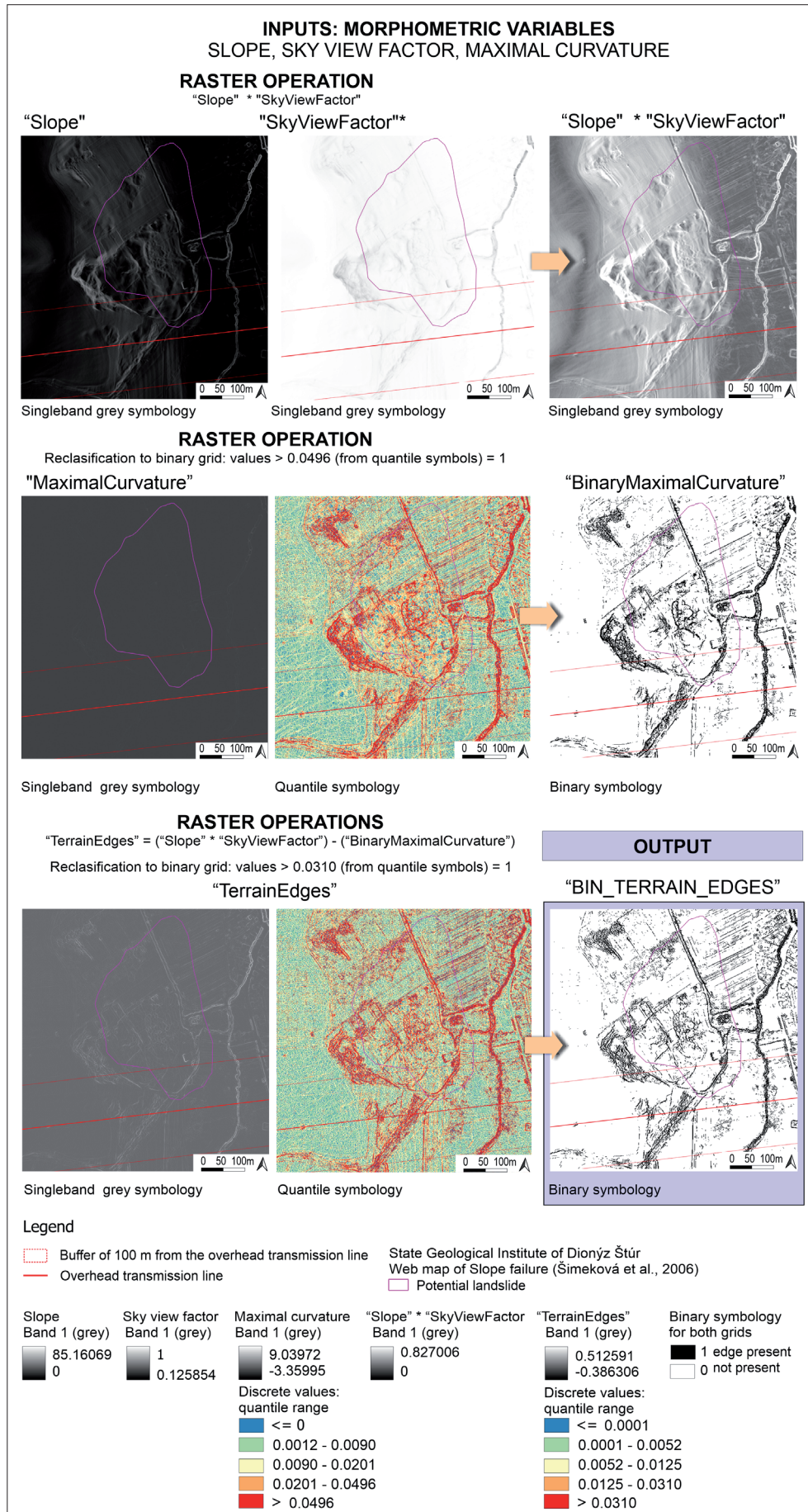


Fig. 3: Site A: process of calculation of a binary grid representing discontinuities in the terrain – terrain edges symbolised with value 1
Source: VUJE a.s.: overhead transmission powerline, poles and protection zone, The Geodesy, Cartography and Cadastre Authority of the Slovak Republic: DMR5.0 (1 m) JTSK(JTSK03), State Geological Institute of Dionýz Štúr: slope failures, modified by the author

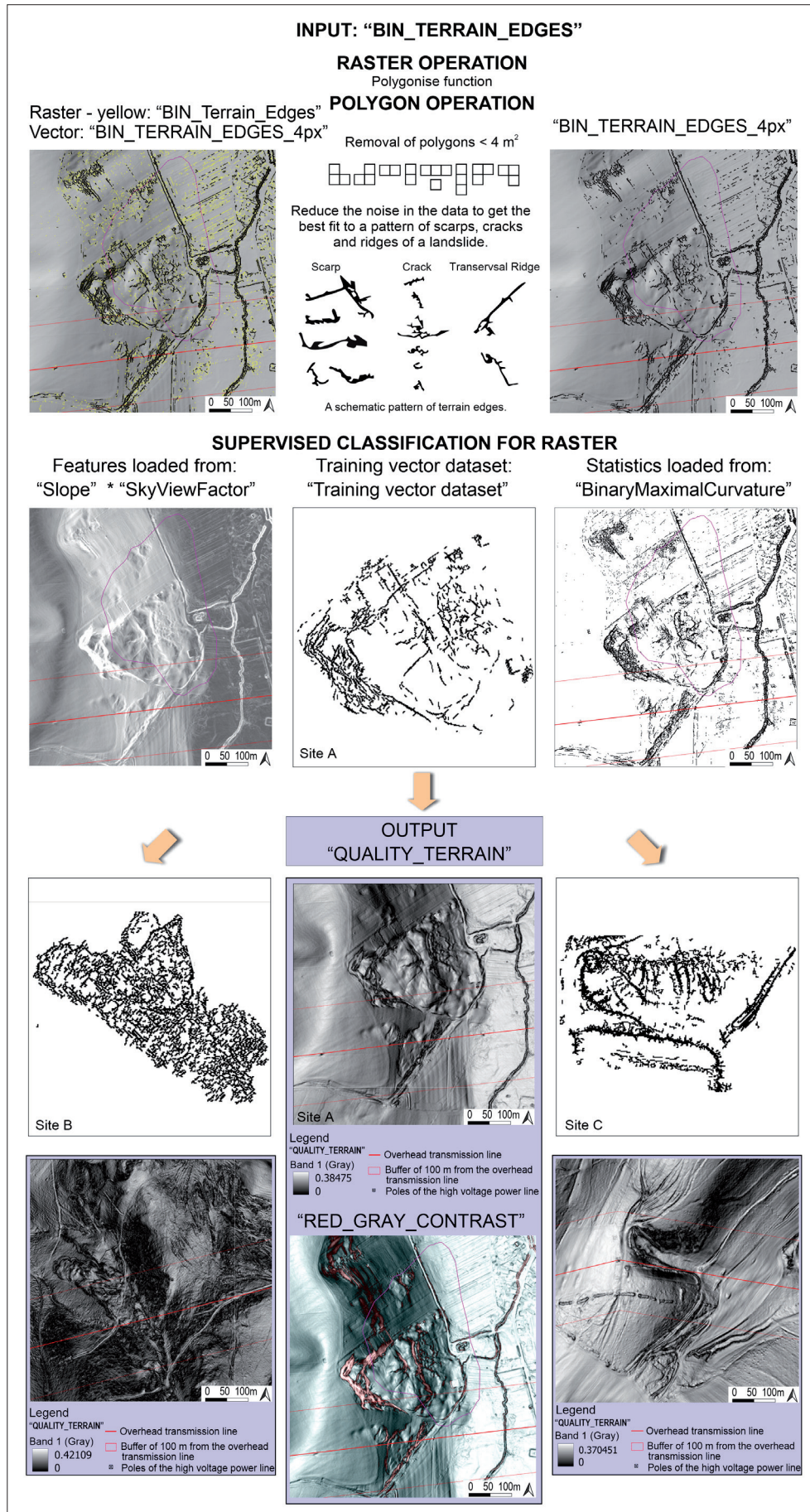


Fig. 4: Site A: process of calculation of a floating-point based grid representing discontinuities in the terrain – terrain edges (upper part). Sites A, B, C: outputs of the supervised classification (lower part)

Source: VUJE a.s.: overhead transmission powerline, poles and protection zone, The Geodesy, Cartography and Cadastre Authority of the Slovak Republic: DMR5.0 (1 m) JTSK(JTSK03), State Geological Institute of Dionýz Štúr: slope failures, modified by the author

Thus, the group of values close to zero represented discontinuities in the terrain – terrain edges on the slopes. These features differed significantly from their surroundings. The classification algorithm categorises them as areas of lower quality due to their uniqueness, higher uncertainty or greater distance from the class centroid within the dataset. On the other side, higher values indicated closer proximity to the centroid and a stronger association with a particular class.

As an experiment, we merged the “QUALITY_TERRAIN” grids from sites A, B and C into a virtual raster (QGIS Python Plugins Repository, 2021) with three separated bands of RGB spectrum. A single virtual layer was a pointer to merged grids. The multi-band symbology of the merged output “RED_GRAY_CONTRAST” visualised terrain edges in contrasting colour – red against other grey-shaded terrain. The symbology settings of the output raster marked the first band as the second and the second and third as the third band of RGB to produce a red-grey colour contrast. Other settings included a normal blend mode, brightness set to 15, gamma set to 1, saturation set to 20 and other parameters left at their default values (Fig. 4).

3.6 Evaluation of terrain edges in derivatives of digital terrain models

3.6.1 Comparison of shadows casted by terrain edges in a hillshade map with QTerrain

Shadows casted by terrain edges were compared within three study sites (A, B and C)

The first, “QUALITY_TERRAIN” raster was examined against a “HILLSHADE” raster and the results were compared and evaluated [ha] per each 25 ha of the study site. Basic unit that was used for evaluation is a pixel of size of one square metre (DMR5.0).

A pseudo formula of the calculation follows:

Sites A, C:

$$((\text{“QUALITY_TERRAIN@1”} >= 0.06) \wedge (\text{“QUALITY_TERRAIN@1”} <= 0.06)) * 1$$

$$((\text{“HILLSHADE@1”} >= 110) \wedge (\text{“HILLSHADE@1”} <= 110)) * 1$$

Site B:

$$((\text{“QUALITY_TERRAIN@1”} >= 0.06) \wedge (\text{“QUALITY_TERRAIN_B@1”} <= 0.06)) * 1$$

$$((\text{“HILLSHADE_B@1”} >= 190) \wedge (\text{“HILLSHADE@1”} <= 190))$$

Reclassification thresholds represent the values of the darkest shadows and were taken as the best result from the experimental testing of the appropriate value.

The second, a longitudinal and a transversal profiles were constructed across each slope failure within the study site. Terrain edges are inherently presented in the “QUALITY_TERRAIN”, while in “HILLSHADE” they were identified using an edge detection algorithm from the SAGA-GIS Wombling Edge Detection module, applied with default parameters (SAGA-GIS Module Library Documentation v2.2.1, 2015). Spatial Wombling is an algorithm used to detect edges in a two-dimensional space (Strydom & Poisot, 2023). Vectorised polygons of terrain edges of “QUALITY_TERRAIN”, and edges detected using the Wombling algorithms in “HILLSHADE” were intersected with a terrain profile created from DMR5.0. The procedure applied qProf plugin 0.5.1 (QGIS Python Plugins Repository, 2023). A length [m] of terrain edges was evaluated.

3.6.2 Evaluation of slope failures and terrain edges along the OHL construction

Slope failures which were difficult to recognise in “HILLSHADE” were additionally digitised using “QUALITY_TERRAIN”. It does

not mean that we were not able to see these subtle landforms in “HILLSHADE” but they did not cast enough strong shadows to identify them as terrain edges.

We compared the number and area [ha] of slope failures identified in “HILLSHADE” and “QUALITY_TERRAIN” and categorised them into three groups: slope failures not requiring field confirmation that were clearly visible in “HILLSHADE”; slope failures not requiring field confirmation that were clearly visible in “QUALITY_TERRAIN”; and slope failures requiring field confirmation. Although terrain edges were present, these were not able to align to typical landslide features defined in Figures 1a and 1b. The presence of all digitised slope failures in the vicinity of the poles of the high-voltage power line was also recorded and evaluated.

BinTE contains more data about possible terrain edges as a binary grid of shadows casted by terrain edges of QT. Therefore, terrain edges were highlighted in BinTE by in red colour to demonstrate a pattern of subtle landforms typical for slope failures for each individual locality. Pattern of subtle landforms typical for slope failures could be used in the future to train a learning machine.

Enumeration of all possible slope failures within the extensive study area was not the primary objective of this article. The results of this methodological step only illustrate the potential applicability of the new method in practice. Graphical outputs of this methodological step are presented in the appendix.

4. Results

4.1 Evaluation of slope failures in a hillshade map

Totally, 22 slope failures was visually identified and manually delineated using “HILLSHADE” in the area along the OHL construction. These were supplemented with slope failures identified in “QUALITY_TERRAIN”. Therefore, are interpreted in a map all together in the further results (4.3).

4.2. Evaluation of terrain edges in a hillshade map compared with QTerrain

Terrain edges are visible in both grid maps based on floating-point data. Undulating terrain and the main scarp are clearly visible in both “HILLSHADE” (Fig. 5 A-I., B-I.) and “QUALITY_TERRAIN” – the product of the new method (Fig. 5 A-II., B-II.). However, the grey scale grid in Figure 5 A-II. and B-II. clearly interprets even small scarps and the contrast in the grey shading depicts undulated terrain in the transport zone of the landslide. The difference is exactly illustrated in the reclassified greyscale maps into binary grids of “HILLSHADE” (Fig. 5 A-III., B-III.) and “QUALITY_TERRAIN” (Fig. 5 A-IV., B-IV.). Shadows casted by terrain edges were present at least twice more in “QUALITY_TERRAIN” against “HILLSHADE” in case of site A (Tab. 2, Fig. 5 A-III. and A-IV.) while about fifty times more of shadows were detected “QUALITY_TERRAIN” against “HILLSHADE” in site B (Tab. 2, Fig. 5 B-III. and B-IV.). Site A exhibited lower difference in the presence of terrain edges shadow evaluated in the “HILLSHADE” and “QUALITY_TERRAIN” against site B (Tab. 2, Figs. 6 and 7). On the other hand, the proposed method had better efficiency on site B where the presence of terrain edges was circa seven times higher in “QUALITY_TERRAIN” against “HILLSHADE” while shadows casted by terrain edges exhibited similar area in both binary grids in case of site A (Tab. 3). Results of site C demonstrating visual comparison are presented the appendix (Appendix 2).

Spatial visualisations created from DMR5.0. of “HILLSHADE” and “QUALITY_TERRAIN” overlapped with ortho-photomosaic of sites A and B demonstrated markedly higher contrast of terrain edges of landslides in “QUALITY_TERRAIN” against

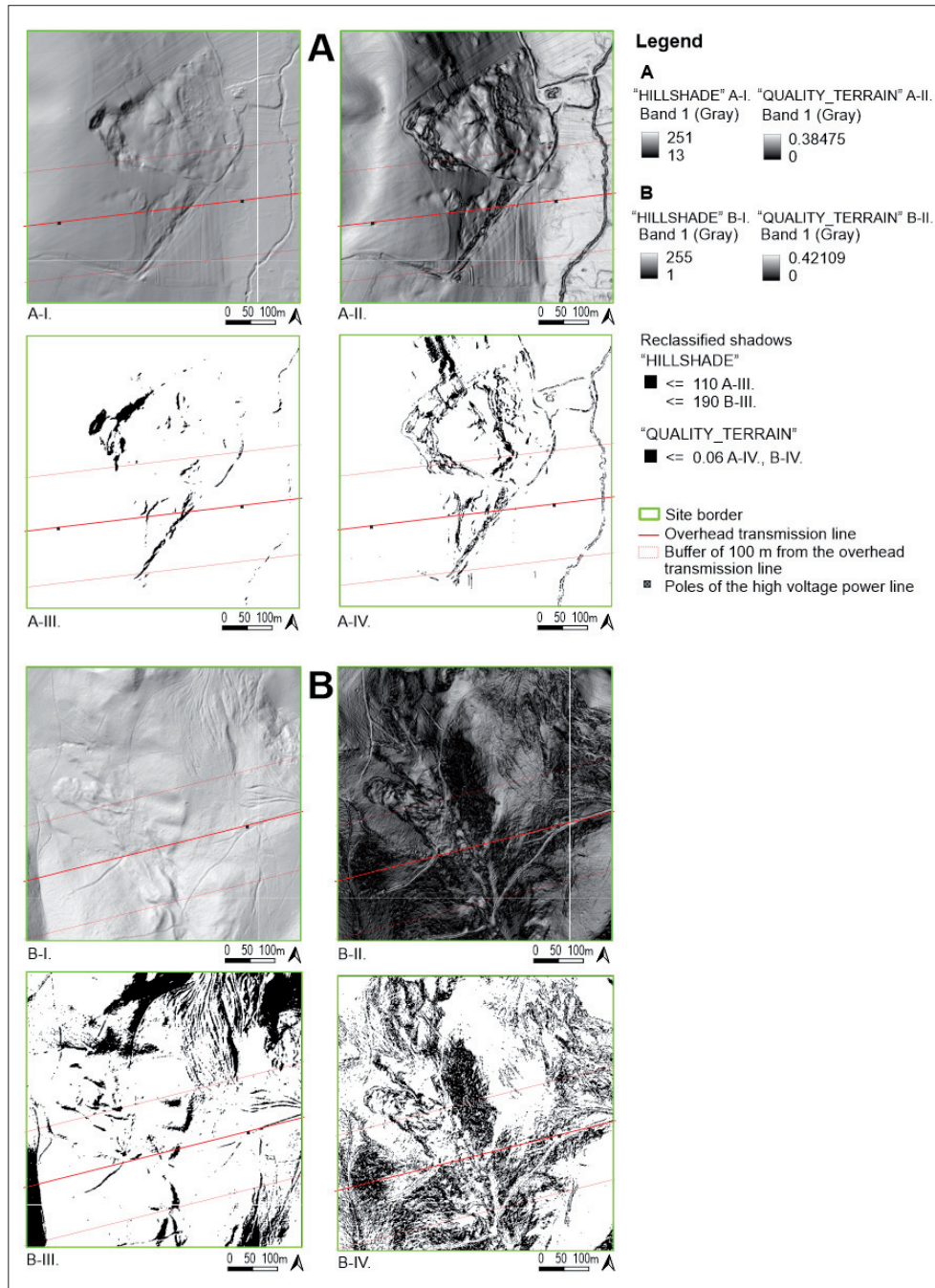


Fig. 5: Comparison between A-I., B-I. – the grayscale grid of “HILLSHADE” and A-II., B-II. – “QUALITY_TERRAIN”. Visual comparison between A-III., B-III. – reclassified grayscale grid to binary grid of “HILLSHADE” and A-IV., B-IV. – reclassified grayscale grid to binary grid of “QUALITY_TERRAIN”

Source: VUJE a.s.: overhead transmission powerline, poles and protection zone, The Geodesy, Cartography and Cadastre Authority of the Slovak Republic: DMR5.0 (1 m) JTSK(JTSK03), State Geological Institute of Dionýz Štúr: slope failures, modified by the author; author’s elaboration: “HILLSHADE”, “QUALITY_TERRAIN”

Site/slope mean	A/9°	B/18°	A/9°	B/18°
Reclassified shadows of edges		[ha]		[%]
“HILLSHADE”: A ≤110 (A-III); B ≤190 (B-III)*	0.52	0.13	2.08	0.52
“QUALITY_TERRAIN”: A (A-IV), B ≤ 0.06 (B-IV)*	1.35	6.62	5.40	26.48
Total area	25	25	100.00	100.00
Wombling filter applied “HILLSHADE” to sum-up terrain edges and “QUALITY_TERRAIN”		[ha]		[%]
“HILLSHADE” (red pixels)	1.96	1.77	7.84	7.08
“QUALITY_TERRAIN” (blue pixels)**	2.41	12.35	9.64	49.40
Total area	25	25	100.00	100.00

Tab. 2: Evaluation of terrain edges in the site area of 25 ha for sites A and B

Notes: *Numbering of sites is adopted from Figure 5; **Figures 6 and 7

Source: Authors’ survey

Site/slope mean	A	B	A	B
Longitudinal terrain profile from edges	[m]		[%]	
“HILLSHADE”	52.00	13.48	17.00	7.88
“QUALITY_TERRAIN”	52.02	96.81	17.00	56.61
Total length	305.96	171	100.00	100.00
Transverse terrain profile from edges	[m]		[%]	
“HILLSHADE” (red pixels)	24.00	5.42	15.68	6.74
“QUALITY_TERRAIN” (blue pixels)	35.01	39.86	22.87	49.54
Total length	153.09	80.46	100.00	100.00

Tab. 3: Evaluation of terrain edges in the terrain profiles of the sites A and B
Source: Authors' survey

“HILLSHADE” also in forest (Appendix 3) and the similar contrast exhibited a gully in site C (Appendix 4). However, rugged terrain and steep slope (18°) made the QTerrain dark and contrast was not so visible in case of site B as we could observe in forest in C with smoother slope (9°). Site A had slope mean parameter the same as site C but a high contrast of slope steepness is visible between the terrain edges of slope failure and the surrounding slopes.

4.3 Evaluation of digitised slope failures a hillshade map enriched with QTerrain data

Slope failures digitised manually in grids of “HILLSHADE” and “QUALITY_TERRAIN” cover an area of 50 ha. In “HILLSHADE” 42 ha of slope failures were identified. Slope failures in an area of 8 ha were additionally detected using “QUALITY_TERRAIN” (Appendix 5). The floating-point based grid of “QUALITY_TERRAIN” highlighted and markedly distinguished these subtle landforms which “HILLSHADE” did

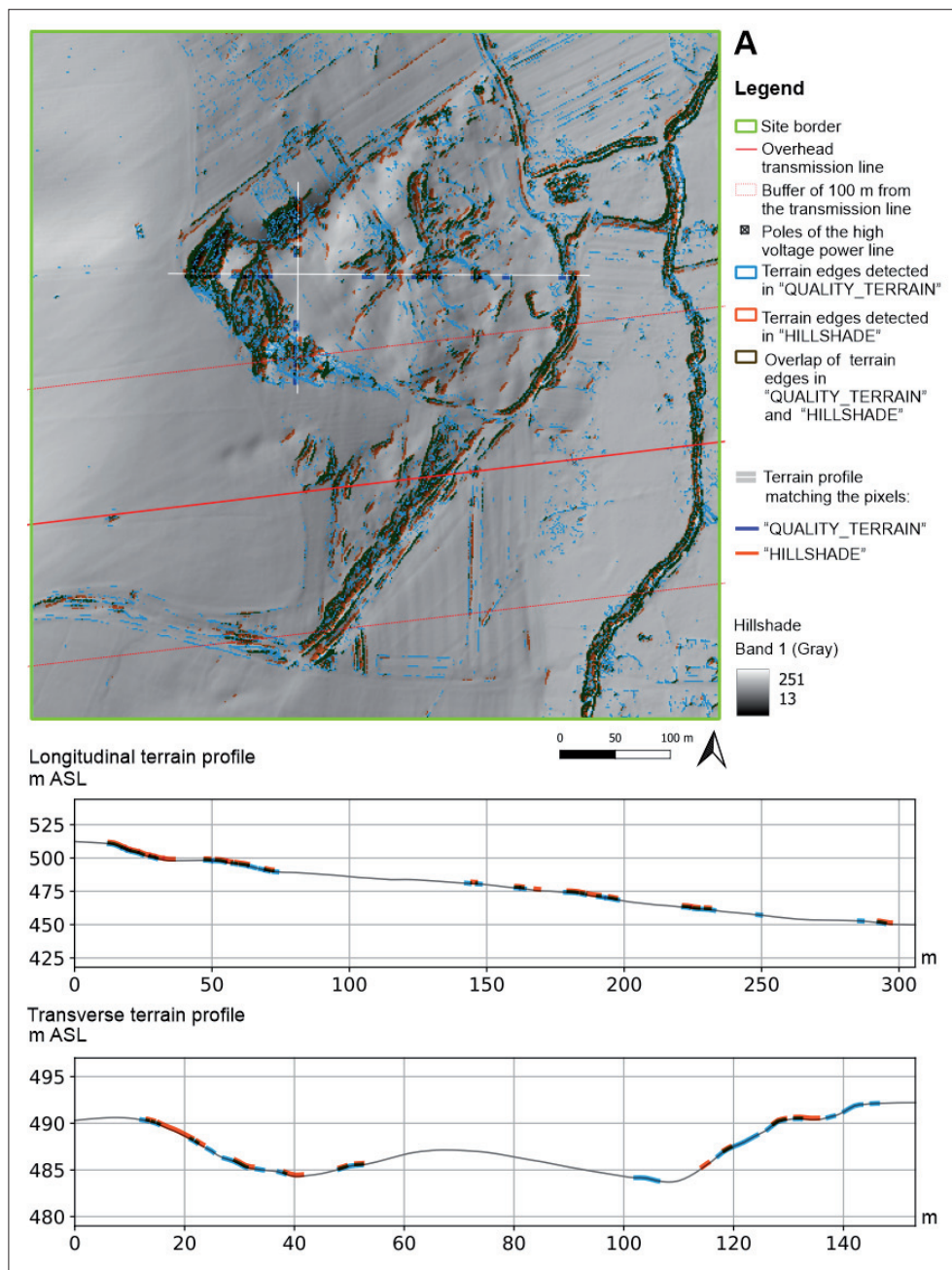


Fig. 6: Site A: Terrain edges evaluated in the grids of “HILLSHADE” and a product of the new method – “QUALITY_TERRAIN”
Source: VUJE a.s.: overhead transmission powerline, poles and protection zone, The Geodesy, Cartography and Cadastre Authority of the Slovak Republic: DMR5.0 (1 m) JTSK(JTSK03), State Geological Institute of Dionýz Štúr: slope failures, modified by the author; author's elaboration: “HILLSHADE”, “QUALITY_TERRAIN”

not illustrate enough, these landforms – features typical for slope failures (explained in Fig. 1) (Appendices 6-1 and 6-2). “BIN_TERRAIN_EDGES” illustrated terrain edges in detail of black-coloured pixels.

In total, 13.5 ha of terrain edges was detected, 11.38 was observed inside the manually digitised polygons from “HILLSHADE” and 2.22 ha from polygons digitised in “QUALITY_TERRAIN”. Slope failures clearly visible in “HILLSHADE” which do not require verification in the field were present on fifteen localities, namely: 4, 6, 7, 9, 10, 11, 12, 13, 14, 15, 17, 19, 20, 21, 22. Other, evidenced in “QUALITY_TERRAIN” were found on two localities, namely: 5QT, 6QT. Then, thirteen have required to be confirmed in the field. Appendices 6-1 and 6-2 demonstrates a pattern of terrain edges (in red) on which basis slope failures are easy to detect. Seven poles of the high voltage power line are located in the polygons of digitised slope failures (3, 6, 8, 9, 11, 13, 15) from which two sites needed to be confirmed in the field (3, 7).

5. Discussion

5.1 Benefits of the new method and challenges for future research

Subtle landforms of terrain edges are a subject of study for variety of landforms such as landslides (Chiba et al., 2008; Korzeniowska et al., 2018; Tarolli et al., 2020), gullies (Na et al., 2017; Yan et al., 2024), cultural terraces (Pijl et al., 2020), roads (Jiao et al., 2021; Slámová et al., 2023), linear structures (Satari & Kazimi, 2021) and many others.

Open-source QGIS tools have opened many possibilities for developing a variety of visualisation techniques and effective procedures are offered through GIS plugins or modules (Tzvetkov, 2018). One such licensed Python module – CSMapper – was developed specifically for landslide detection. It's released under the GNU Public License (GPL) Version 2 and authorised by Kosuke Asahi (QGIS Python Plugins

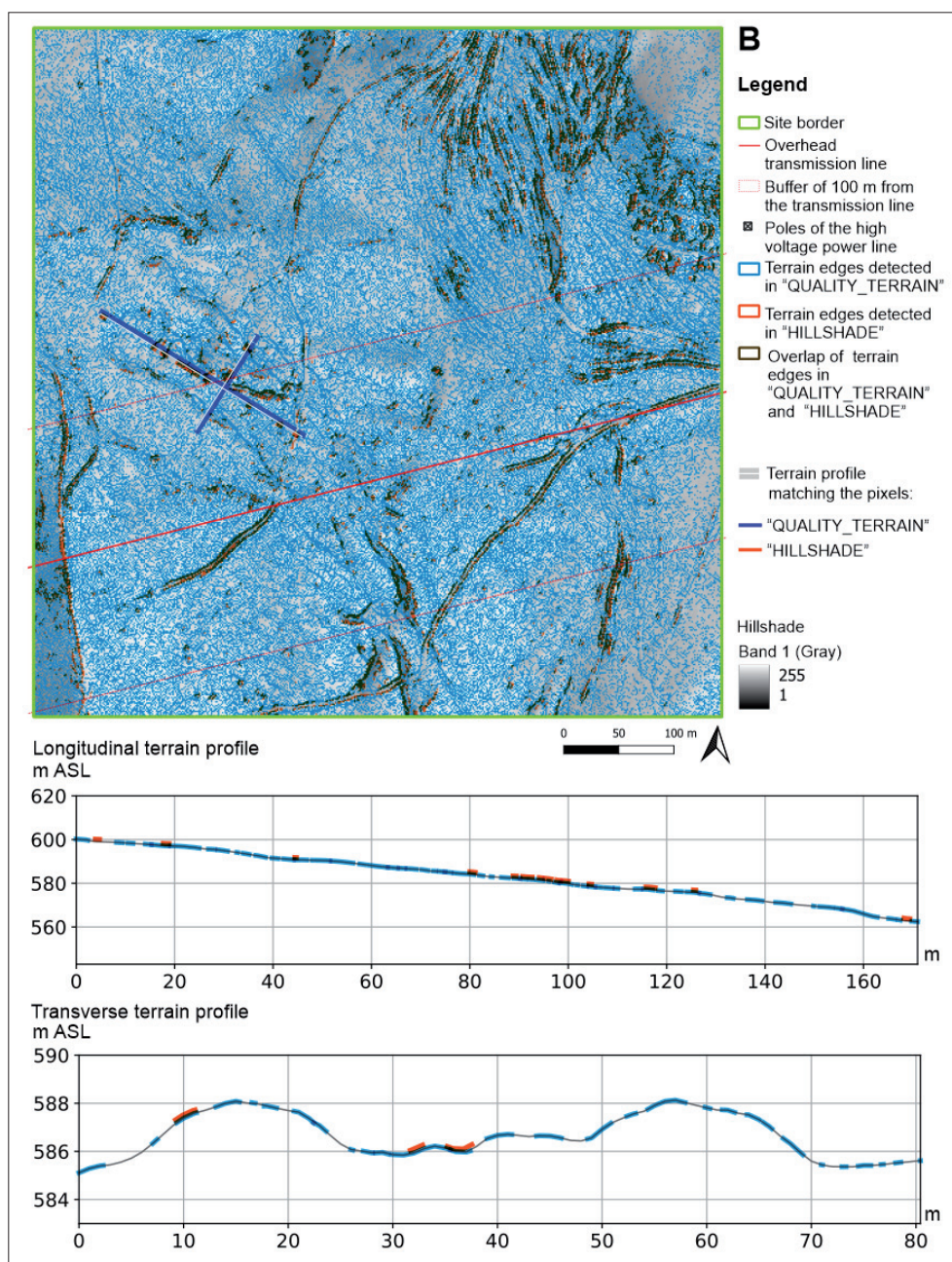


Fig. 7: Site B: Terrain edges evaluated in the grids “HILLSHADE” and a product of the new method – “QUALITY_TERRAIN”
Source: VUJE a.s.: overhead transmission powerline, poles and protection zone, The Geodesy, Cartography and Cadastre Authority of the Slovak Republic: DMR5.0 (1 m) JTSK(JTSK03), State Geological Institute of Dionýz Štúr: slope failures, modified by the author; author's elaboration: “HILLSHADE”, “QUALITY_TERRAIN”

Repository, 2019). This module enables the identification of landslides based on a red relief image map (RRIM) and colour contrast formed by terrain edges visualised by superimposing different derivatives of a digital terrain model (Chiba et al., 2008; Chiba & Hasi, 2016). A first comparison between RRIM outputs and landslides detected using a binary raster of terrain edges introduced Chudý et al. (2019).

RRIM is a set of superimposed grid maps, not a single raster. The outputs of the newly developed method are: the binary grid of BinTerrain (“BIN_TERRAIN_EDGES”) (Fig. 3), the grey scaled grid of QTerrain (“QUALITY_TERRAIN”) and its red-grey coloured modification “RED_GRAY_CONTRAST” (Fig. 4). The advantage of interpreting terrain edges in a single grid map over RRIM lies in the potential for further processing using raster-based operations.

The advantages of the pixel-based method lie in the number of GIS tools readily available and usable for operations on the pixel raster intended for digital terrain models, even for the common user. Logical and arithmetic operations, classification, overlay, and fusion of images derived from detailed digital models can yield derivatives applicable across various scientific disciplines, such as archaeology (Kokalj & Somrak, 2019; Štular et al., 2012), geomorphology for slope deformation indications (Pirotti & Tarolli, 2010; Guzzetti et al., 2012; Peternel et al., 2017; Chudý et al., 2019; Jagodnik et al., 2020), applied ecology (Leempoel et al., 2015), or environmental history (Lieskovský et al., 2022). Combining land cover structures with quasi-3D relief raster files, such as overlapping slope, topographic openness, and multidirectional hillshade, proves valuable in visualising the topographic pattern of slope failures, even in the case of older landslides (Lee et al., 2017).

Easy transfer between raster and vector forms enables simple measurements of slope movements. Measuring is important to monitor slope failure activity (Lucieer et al., 2014) and it can be achieved using multi-temporal LiDAR digital terrain models (Anders et al., 2013). Binary interpretation of terrain edges pixels in the grid makes it possible to identify, delimit and finally evaluate their area or length as we documented on the study sites. Terrain edges of slope failures appeared more frequently and on more extensive area in “QUALITY_TERRAIN” as it was in “HILLSHADE” grid (Tabs. 2 and 3; Figs. 5, 6 and 7; Appendix 2). The visual prominence of the outputs of the newly developed method supports also spatial visualisations of “HILLSHADE” and “QUALITY_TERRAIN” overlapped with ortho-photomosaic. QTerrain exhibited markedly higher contrast in overlaid layers with agricultural and forest landscape against hillshade map (Appendices 3 and 4).

Manual digitising of subtle landforms in an extensive area would be time consuming and inefficient. The hillshade map does not provide interpretation of terrain edges in such a detail as QTerrain as shown at sites 1QT–8QT (Appendices 6-1 and 6-2). A user may unintentionally overlook and omit landslides with indistinct terrain edges which do not cast sufficient shadows in the hillshade map. Jaboyedoff et al. (2018) found that not all slope failures can be identified in digital derivatives of DTM. We found slightly less than half (13 sites) of their total number that would need to be confirmed in the field survey.

Regarding the extensive area along the OHL construction, we are aware of the spatial discontinuity of the investigated slope failures. The reason for the selection was the project objective to identify slope failures in this area using an innovative method. An actual challenge is to perform field measurements of terrain edges in the transects of site A and B using professional GNSS (Chudý et al., 2018a, b, Chudý et al., 2019) and adopt a method by Du et al. (2023) to evaluate correspondence or divergence of data digitally computed in the transects with data measured in the

field. Based on the results we would be able to identify: correctly computed terrain edges, false positives (non-existent edges) and false negatives (missing edges). Further, this comparison would suggest which output of the new method BinTerrain or QTerrain could be more suitable to generate a pattern of landslide features. Geometric pattern consisting of geometric shapes (Fig. 4 and Appendices 6-1 and 6-2) derived from binary interpretation of terrain edges would be employed to automate detection and inventorying landslides on a landscape scale. Pixel-based terrain variables thresholds allow easy and flexible adapt the same diagnostic terrain variables as predictive inputs to machine learning models (Brecheisen & Richter, 2021; Masruroh et al., 2023).

5.2 Applicability of the method

A prospective model for landslide mapping and monitoring is predicated upon the utilisation of multiscale and multitemporal spatially referenced data from a diverse array of sources (Hou et al., 2017). A geomorphometric analysis of slope failures and their selected features derived from disparate data sources on different scales enables the identification and categorisation of multiscale components of slope failures (Mora et al., 2018). The classification of landforms is inherently scale-sensitive as, for instance, the Topographic Position Index demonstrates (Giano et al., 2020). DTMs of different resolutions contain different topographic information, resulting in variations in the spatial distribution of terrain parameters on different scales, which has a significant impact on the spatial distribution of calculated parameters such as slope and water flow distribution (Thomas et al., 2017). The new method showed its robustness when it was applied on three different resolutions of DTMs and multiscale application was demonstrated on site C (Appendix 7). We compared “HILLSHADE” and “QUALITY_TERRAIN” at three resolutions of DTM: 10 m, 1 m and 0.15 m per pixel. The most obvious difference was in DMR3.5 between “QUALITY_TERRAIN” and “HILLSHADE” in which the shape of the gully was difficult to recognise. DMR5.0 distinctly depicted slope failure features such as scarps, tension cracks, and transverse ridges, among others. While DMR3.5 lacked the resolution necessary to detect subtle landforms, on the other side, general shape of a gully was markedly visible. Thus, lower resolution DTMs could be helpful to indicate erosion objects or sliding slopes over extensive areas, on a landscape scale. In contrast to lower resolutions, extra dense LiDAR with the average point density of 254 PPSM per ground was used. It demonstrated the potential to complement the DMR5.0 data, visualising subtle landforms in intrinsic detail even in forests with dense tree canopy and shrub stage, rugged terrain, deep valleys, ravines or gullies with steep slopes which make obstacles for penetration of laser.

Forest has many limitations for aerial LiDAR or photogrammetry (Van Den Eeckhaut et al., 2007). LiDAR appears to be more suitable than photogrammetry for mapping subtle landforms due to its ability to penetrate dense canopies, whereas photogrammetry often leaves many data gaps (Chudý et al., 2018a,b). More detailed data can be collected using hyperspectral sensors. These can provide exceptionally detailed spectral surface reflectance data, but their processing, especially from airborne cameras, requires complex corrections, making them difficult to use for terrain mapping (Jakob et al., 2017). The fusion of extra dense LiDAR with selected indices from hyperspectral data could help to explore relationships between vegetation and subtle landforms (Demarchi et al., 2020). However, high-resolution digital models are beneficial for extracting target topography only when the model accurately represents well-defined terrain morphology (Sofia et al., 2010).

The presence of slope failures on different slope grades (DMR5.0) in the area along the OHL construction was indicated according to terrain edges calculated from “BIN_TERRAIN_

EDGES". More than half of their total amount inside the digitised polygons of slope failures was found on slopes steeper than 15° (7.13 ha); 4.45 ha was within the interval from 15° to 25° what aligns with findings from other authors (Zęzere, 2002; Frattini et al., 2004) and 2.68 ha was found above 25° (Appendix 5). Initially, we assumed that the usability of BinTerrain or QTerrain on slopes above 25° might be limited due to the low contrast between the subtle landforms of slope failures and other landforms in their vicinity. Terrain edges of QTerrain casted more shadows in case of site B with slope mean 18° against site A with slope mean 9°. In site B, QTerrain exhibited circa seven times higher presence of shadows against the hillshade map (Tabs. 2 and 3, Figs. 5, 6 and 7).

6. Conclusions

While contactless technologies have a wide range of applications, their limitations lie in data quality, processing time and financial investment. The most efficient dataset in the research was considered to be DMR5.0. Results demonstrated that binary and grey shaded grid derivatives had sufficient resolution to visualise even subtle landforms which may indicate initial phases of the slope movement.

The main benefit of the proposed method is seen in the interpretation of the pattern of terrain edges which is typical for slope failures. Discrete interpretation BinTerrain – "BIN_TERRAIN_EDGES" exactly shows terrain edges with a certain resolution given by the DTM. Binary patterns of different types of slope failures could be used as training datasets for machine learning algorithms in future research. In comparison, manually digitised polygons are subjectively vectorised and borders suffer for lack of details. Application of these polygons of slope failures as training datasets based on grid in machine learning is questionable. Here, exact binary interpretation of terrain edges would bring more accurate results.

The main advantage of QTerrain's floating-point grid is that it enhances the contrast of terrain edges, making them easy to recognise even in large areas on a landscape scale. Coloured interpretation of QTerrain is comparable with known RRIM raster that is the algorithm used to detect terrain edges of failed slopes. Applicability of the method across different resolutions of DTMs makes it flexible to use on different geographic scales which are relevant for mapping of terrain edges.

Terrain edges casted more shadows in QTerrain than in the hillshade map and the most visible difference was on steeper slopes (site B, 18°) while moderate slopes (A, 9°) have not exhibited so contrasting presence of shadow casted by terrain edges between the hillshade map and QTerrain. Moreover, as slope failures predominantly occur on slopes above 15°, these slopes are often covered with shrubs or forest. Floating-point base grid of QTerrain allows clear and sharp visualisation of terrain. Identification of subtle terrain edges in visualisations combining terrain and real land cover – orthophotomosaic is easier than in the hillshade map overlapped with land cover.

Acknowledgement

This publication is the result of the project implementation: Research on the application of artificial intelligence tools in the analysis and classification of hyperspectral sensing data (ITMS: NFP313011BWC9) supported by the Operational Programme Integrated Infrastructure (OPII) funded by the ERDF. The Authors gratefully acknowledge the contribution of the Slovak Research and Development Agency under the project APVV-23-0289 OPEREL "Increasing the operational reliability of linear power structures by using data from remote sensing".

References:

- Abellan, A., Derron, M. H., & Jaboyedoff, M. (2016). Use of 3D Point Clouds in Geohazards Special Issue: Current Challenges and Future Trends. *Remote Sensing*, 8, 130. <https://doi.org/10.3390/rs8020130>
- Aigbadon, G. O., Ocheli, A., & Akudo, E. O. (2021). Geotechnical evaluation of gully erosion and landslides materials and their impact in Iguosa and its environs, southern Nigeria. *Environmental Systems Research*, 10, 36. <https://doi.org/10.1186/s40068-021-00240-6>
- Alliez, P., Meyer, M., & Desbrun, M. (2002). Interactive geometry remeshing. *ACM Transactions on Graphics*, 21(3), 347–354. <https://dl.acm.org/doi/10.1145/566654.566658>
- Al-Rawabdeh, A., He, F., Moussa, A., El-Sheimy, N., & Habib, A. (2016). Using an Unmanned Aerial Vehicle-Based Digital Imaging System to Derive a 3D Point Cloud for Landslide Scarp Recognition. *Remote Sensing*, 8, 95. <https://doi.org/10.3390/rs8020095>
- Anders, N. S., Seijmonsbergen, A. C., & Bouten, W. (2013). Geomorphological Change Detection Using Object-Based Feature Extraction from Multi-Temporal LiDAR Data. *IEEE Geoscience and Remote Sensing Letters*, 10(6), 1587–1591. <https://doi.org/10.1109/LGRS.2013.2262317>
- ARCGISpro (2023). Compute Change Raster (Image Analyst). <https://pro.arcgis.com/en/pro-app/3.0/tool-reference/image-analyst/compute-change-raster.htm>
- Azizi, Z., Najafi, A., & Sadeghian, S. (2014). Forest Road Detection Using LiDAR Data. *Journal of Forestry Research*, 25, 975–980. <https://doi.org/10.1007/s11676-014-0544-0>
- Barbosa, N., Andreani, L., Gloaguen, R., & Ratschbacher, L. (2021). Window-Based Morphometric Indices as Predictive Variables for Landslide Susceptibility Models. *Remote Sensing*, 13, 451. <https://doi.org/10.3390/rs13030451>
- Berti, M., Corsini, A., & Daehne, A. (2013). Comparative analysis of surface roughness algorithms for the identification of active landslides. *Geomorphology*, 182, 1–18. <https://doi.org/10.1016/j.geomorph.2012.10.022>. <https://doi.org/10.1016/j.geosciences.2012.10.022>
- Brecheisen, Z. S., & Richter, D. (2021). Gully-erosion estimation and terrain reconstruction using analyses of microtopographic roughness and LiDAR. *Catena*, 202, 105264. <https://doi.org/10.1016/j.catena.2021.105264>
- British Geological Survey (2024). How to classify a landslide. <https://www.bgs.ac.uk/discovering-geology/earth-hazards/landslides/how-to-classify-a-landslide/>
- Cesar, R. M., & Costa, L. D. F. (1995). A Pragmatic Introduction to Machine Vision, by R. Jain, R. Kasturi and B. G. Schunck. *Real Time Imaging*, 1(6), 437–439. <https://doi.org/10.1006/rtim.1995.1045>
- Chiba, T., & Hasi, B. (2016). Ground surface visualization using red relief image map for a variety of map scales. *International Archives of the Photogrammetry Remote Sensing and Spatial Information Sciences*, 41, 393–397. <https://doi.org/10.5194/isprs-archives-XLI-B2-393-2016>
- Chiba, T., Kaneta, S., & Suzuki, Y. (2008). Red Relief Image Map, New Visualization Method for Three Dimensional Data. *International Archives of the Photogrammetry Remote Sensing and Spatial Information Sciences*, 37, 1071–1076. https://www.isprs.org/proceedings/XXXVII/congress/2_pdf/11_ThS-6/08.pdf
- Chudý, F., Sadibol, J., Slamova, M., Belacek, B., Beljak Pazinova, N., & Beljak, J. (2018b). Identification of Historic Roads in the Forest Landscape by Modern Contactless Methods of Large-Scale Mapping. In: *Geoconference on Informatics, Geoinformatics and Remote Sensing* (pp. 183–190). Book Series: International Multidisciplinary GeoConference-SGEM, Albena Bulgaria.
- Chudý F., Slámová, M., Tomašík, J., Prokešová, R., & Mokroš, M. (2019). Identification of Micro-Scale Landforms of Landslides Using Precise Digital Elevation Models. *Geosciences*, 9(3), 117. <https://doi.org/10.3390/geosciences9030117>
- Chudý, F., Slámová, M., Tomašík, J., Tunák, D., Kardoš, M., & Saloň, Š. (2018a). The application of civic technologies in a field survey of landslides. *Land Degradation & Development*, 29(6), 1858–1870. <https://doi.org/10.1002/ldr.2957>
- Cruden, D. M., & Varnes, D. J. (1996). Landslide types and processes. In A. K. Turner, & R. L. Schuster (Eds.), *Landslides investigation and mitigation*. Transportation Research Board, Special Report No. 247, U.S. National Research Council.

- Demarchi, L., Kania, A., Ciężkowski, W., Piórkowski, H., Oświecimka-Piasko, Z., & Chormański, J. (2020). Recursive Feature Elimination and Random Forest Classification of Natura 2000 Grasslands in Lowland River Valleys of Poland Based on Airborne Hyperspectral and LiDAR Data Fusion. *Remote Sensing*, 12, 1842. <https://doi.org/10.3390/rs12111842>
- Đlugosz, M. (2012). Digital Terrain Model (DTM) as a Tool for Landslide Investigation in the Polish Carpathians. *Studia Geomorphologica Carpatho-Balcanica* 2012, XLVI, 5–23. <https://doi.org/10.2478/v10302-012-0001-3>
- Domènech, G., Alvioli, M., & Corominas, J. (2019). Preparing first-time slope failures hazard maps: From pixel-based to slope unit-based. *Landslides*, 17, 249–265. <http://doi.org/10.1007/s10346-019-01279-4>
- Du, P., Xu, Y., Guo, Y., & Li, H. (2023). Assessing loess landslide volume using high-precision UAV-derived DEM: A case study of the 15 March 2019 landslide in Zaoling Township, Xiangning County in North China. *Natural Hazards Research*, 3(4), 640–645. <https://doi.org/10.1016/j.nhres.2023.07.006>
- Evans, I. S., & Cox, N. J. et al. (1999). Relations between land surface properties: altitude, slope and curvature. In S. Hergarten, & H. J. Neugebauer (Eds.), *Process Modelling and Landform Evolution*, Vol. 78 (pp. 13–45). Springer. <https://doi.org/10.1007/BFb0009718>
- Fernández, T., Pérez, J. L., Colomo, C., Cardenal, J., Delgado, J., Palenzuela, J. A., ..., & Chacón, J. (2017). Assessment of the Evolution of a Landslide Using Digital Photogrammetry and LiDAR Techniques in the Alpujarras Region (Granada, Southeastern Spain). *Geosciences*, 7(2), 32. <https://doi.org/10.3390/geosciences7020032>
- Frattoni, P., Crosta, G. B., Fusi, N., & Dal Negro, P. (2004). Shallow landslides in pyroclastic soil: a distributed modelling approach for hazard assessment. *Engineering Geology*, 73, 277–295. <https://doi.org/10.1016/j.enggeo.2004.01.009>
- Giano, S. I., Danese, M., Gioia, D., Pescatore, E., Siervo, V., & Bentivenga, M. (2020). Tools for Semi-automated Landform Classification: A Comparison in the Basilicata Region (Southern Italy). In O. Gervasi et al. (Eds.), *Computational Science and Its Applications – ICCSA 2020*. ICCSA 2020. Lecture Notes in Computer Science, Vol. 12250 (pp. 709–722). Springer. https://doi.org/10.1007/978-3-030-58802-1_51
- Giordan, D., Adams, M. S., Aicardi, E., Alicandro, M., Allasia, P., Baldo, M., ..., & Troilo, F. (2020). The use of unmanned aerial vehicles (UAVs) for engineering geology applications. *Bulletin of Engineering Geology and the Environment* 79, 3437–3481. <https://doi.org/10.1007/s10064-020-01766-2>
- GISGeography, 2023. Quantile Classification in GIS. <https://gisgeography.com/quantile-classification-gis/>
- Guthrie, R. H., & Evans, S. G. (2004). Magnitude and frequency of landslides triggered by a storm event, Loughborough Inlet, British Columbia. *Natural Hazards and Earth System Science*, 4(3), 475–483. <https://nhess.copernicus.org/articles/4/475/2004/nhess-4-475-2004.pdf>
- Guzzetti, F., Mondini, A. C., Cardinali, M., Fiorucci, F., Santangelo, M., & Chang, K.-T. (2012). Landslide inventory maps: New tools for an old problem. *Earth-Science Reviews*, 112, 42–66. <http://dx.doi.org/10.1016/j.earscirev.2012.02.001>
- Harris, A., & Baird, A. J. (2018). Microtopographic Drivers of Vegetation Patterning in Blanket Peatlands Recovering from Erosion. *Ecosystems*, 1–20. <https://doi.org/10.1007/s10021-018-0321-6>
- Hou, W., Lu, X., Wu, P., Xue, A., & Li, L. (2017). An Integrated Approach for Monitoring and Information Management of the Guanling Landslide (China). *ISPRS International Journal of Geo-Information*, 6, 79. <https://doi.org/10.3390/ijgi6030079>
- Hussain, M., Chen, D., Cheng, A., Wei, H., & Stanley, D. (2013). Change detection from remotely sensed images: From pixel-based to object-based approaches. *ISPRS Journal of Photogrammetry and Remote Sensing*, 80, 91–106. <http://dx.doi.org/10.1016/j.isprsjprs.2013.03.006>
- Jaboyedoff, M., Abellán, A., Carrea, D., Derron, M. H., Matasci, B., & Michoud, C. (2018). Mapping and monitoring of landslides using LiDAR. In R. Singh, & D. Bartlett (Eds.), *Natural Hazards* (pp. 397–420). CRC Press. <https://doi.org/10.1201/9781315166841-17>
- Jagodnik, P. (2024). Evaluating the potential of visual interpretation of airborne LiDAR datasets for the identification and mapping of small landslides. In EGU General Assembly 2024, Vienna, Austria, 14–19 Apr 2024, EGU24-15211. <https://doi.org/10.5194/egusphere-egu24-15211>
- Jagodnik, P., Jagodnik, V., Arbanas, Ž., & Mihalčić Arbanas, S. (2020). Landslide types in the Slani Potok gully, Croatia. *Geologia Croatica*, 73, 13–28. <https://doi.org/10.4154/gc.2020.04>
- Jakob, S., Zimmermann, R., & Gloaguen, R. (2017). The Need for Accurate Geometric and Radiometric Corrections of Drone-Borne Hyperspectral Data for Mineral Exploration: MEPHYSTo – A Toolbox for Pre-Processing Drone-Borne Hyperspectral Data. *Remote Sensing*, 9, 88. <https://doi.org/10.3390/rs9010088>
- Jasiewicz, J., & Stepinski, T. F. (2013). Geomorphons – a pattern recognition approach to classification and mapping of landforms. *Geomorphology*, 182, 147–156. <https://doi.org/10.1016/j.geomorph.2012.11.005>
- Jiao, C., Heitzler, M., & Hurni, L. (2021). A survey of road feature extraction methods from raster maps. *Transactions in GIS*, 25, 2734–2763. <https://doi.org/10.1111/tgis.12812>
- Kampouraki, M., Wood, G. A., & Brewer, T. R. (2008). Opportunities and limitations of object based image analysis for detecting urban impervious and vegetated surfaces using true-colour aerial photography. In T. Blaschke, S. Lang, & G. Hay (Eds.), *Object-Based Image Analysis-Spatial Concepts for Knowledge-Driven Remote Sensing Applications* (pp. 555–569). Springer. https://doi.org/10.1007/978-3-540-77058-9_30
- Kokalj, Ž., & Somrak, M. (2019). Why Not a Single Image? Combining Visualizations to Facilitate Fieldwork and On-Screen Mapping. *Remote Sensing*, 11(7), 747. <https://doi.org/10.3390/rs11070747>
- Korzeniowska, K., Pfeifer, N., & Landtwinig, S. (2018). Mapping Gullies, Dunes, Lava Fields, and Landslides via Surface Roughness. *Geomorphology*, 301, 53–67. <http://doi.org/10.1016/j.geomorph.2017.10.011>
- LAStools, 2023. LAStools. <http://rapidlasso.com/LAStools>
- Lee, C. F., Huang, W. K., Huang, C. M., & Chi, C. C. (2017). Deep-seated landslide mapping and geomorphic characteristic using high resolution DTM in northern Taiwan. In *Workshop on World Landslide Forum* (pp. 767–777). Springer. https://doi.org/10.1007/978-3-319-53498-5_88
- Leempoel, K., Parisod, Ch., Geiser, C., Daprà, L., Vittoz, P., & Joost, S. (2015). Very high-resolution digital elevation models: Are multi-scale derived variables ecologically relevant? *Methods Ecology and Evolution*, 6, 1373–1383. <https://doi.org/10.1111/2041-210X.12427>
- Li, G., & Wan, Y. (2015). A new combination classification of pixel- and object-based methods. *International Journal of Remote Sensing*, 36(23), 5842–5868. <https://doi.org/10.1080/01431161.2015.1109728>
- Lieskovský, J., Lieskovský, T., Hladíková, K., Štefunková, D., & Hurajtová, N. (2022). Potential of airborne LiDAR data in detecting cultural landscape features in Slovakia. *Landscape Research*, 47(5), 539–558. <https://doi.org/10.1080/01426397.2022.2045923>
- Liščák, P., Paudiš, P., Petro, L., Iglárová, E., Ondrejka, P., Dananaj, I., ..., & Drotár, D. (2010). Registration and evaluation of newly evolved slope failures in 2010 in Prešov and Košice regions. *Mineralia Slovaca*, 42(2), 393–406.
- Liu, D., & Xia, F. (2010). Assessing object-based classification: advantages and limitations. *Remote Sensing Letters*, 1(4), 187–194. <https://doi.org/10.1080/01431161003743173>
- Liu, S., Yin, K., Zhou, C., Gui, L., Liang, X., Lin, W., & Zhao, B. (2021). Susceptibility Assessment for Landslide Initiated along Power Transmission Lines. *Remote Sensing*, 13(24), 5. <https://doi.org/10.3390/rs13245068>
- Lucieer, A., Jong, S. M. de, & Turner, D. (2014). Mapping landslide displacements using Structure from Motion (SfM) and image correlation of multi-temporal UAV photography. *Progress in Physical Geography: Earth and Environment*, 38(1), 97–116. <http://dx.doi.org/10.1177/0309133313515293>
- Maglay, J., Moravcová, M., Šefčík, P., Vlačíky, M., & Pristaš, J. (2011). Prehľadná geologická mapa kvartéru Slovenskej republiky 1:200,000. Bratislava (The Ministry of the Environment and State Geological Institute of Dionýz Štúr – SGIDŠ) <https://www.geology.sk/prehľadne-geologicke-mapy-v-mierke-1-200-000/>
- Mărgărint, M. C., & Niculiță, M. (2017). Landslide Type and Pattern in Moldavian Plateau, NE Romania. In M. Radoane, & A. Vespremeanu-Stroe (Eds.), *Landform Dynamics and Evolution in Romania* (pp. 271–304). Springer. https://doi.org/10.1007/978-3-319-32589-7_12
- Martins, B. H., Suzuki, M., Yastika, P. E., & Shimizu, N. (2020). Ground Surface Deformation Detection in Complex Landslide Area—Bobonaro, Timor-Leste—Using SBAS DInSAR, UAV Photogrammetry, and Field Observations. *Geosciences*, 10, 245. <https://doi.org/10.3390/geosciences10060245>
- Mašlár, E., Mašárová, I., Ondrus, P., Jelínek, R., Stercz, M., Pačajová, K., & Stašik, L. (2020). Engineering geological investigations of slope

- deformations at selected localities in the period 2018–2019. *Geologické práce, Správy* 136, 19–32. https://www.geology.sk/wp-content/uploads/documents/foto/GPS/136/02-Maslar_GPS_136.pdf
- Masruroh, H., Soemarno, S., Kurniawan, S., & Leksono, A. S. (2023). A Spatial Model of Landslides with A Micro-Topography and Vegetation Approach for Sustainable Land Management in the Volcanic Area. *Sustainability*, 15, 3043. <https://doi.org/10.3390/su15043043>
- Mayoral, A., Toumazet, J.-P., Simon, F.-X., Vautier, F., & Peiry, J.-L. (2017). The Highest Gradient Model: A New Method for Analytical Assessment of the Efficiency of LiDAR-Derived Visualization Techniques for Landform Detection and Mapping. *Remote Sensing*, 9, 120. <https://doi.org/10.3390/rs9020120>
- Mercuri, M., Conforti, M., Ciurleo, M., & Borrelli, L. (2023). UAV Application for Short-Time Evolution Detection of the Vomice Landslide (South Italy). *Geosciences*, 13(2), 29. <https://doi.org/10.3390/geosciences13020029>
- Ministry of the Environment of the Slovak Republic (2018). Program prevencie a manažmentu zosuvných rizík (2014–2020) – aktualizácia. <https://www.minzp.sk/files/sekcia-geologie-prirodných-zdrojov/program-prevencie-manazmentu-zosuvných-rizík-2014-2020-aktualizacia.pdf>
- Mora, O. E., Lenzano, M. G., Toth, C. K., Grejner-Brzezinska, D. A., & Payne, J. V. (2018). Landslide Change Detection Based on Multi-Temporal Airborne LiDAR-Derived DEMs. *Geosciences*, 8, 23. <https://doi.org/10.3390/geosciences8010023>
- Na, J., Yang, X., Dai, W., Li, M., Xiong, L., Zhu, R., & Tang, G. (2017). Bidirectional DEM relief shading method for extraction of gully shoulder line in loess tableland area. *Physical Geography*, 39, 368–386. <https://doi.org/10.1080/02723646.2017.1410974>
- Ortuño, M., Guinau, M., Calvet, J., Furdada, G., Bordonau, J., Ruiz, A., & Camafort, M. (2017). Potential of airborne LiDAR data analysis to detect subtle landforms of slope failure: Portainé, Central Pyrenees. *Geomorphology*, 295, 364–382. <https://doi.org/10.1016/j.geomorph.2017.07.015>
- Parkner, T., Page, M. J., Marden, M., & Marutani, T. (2007). Gully systems under undisturbed indigenous forest, East Coast Region, New Zealand. *Geomorphology*, 84, 241–253. <https://doi.org/10.1016/j.geomorph.2006.01.042>
- Peternel, T., Kumelj, Š., Oštir, K., & Komac, M. (2017). Monitoring the Potoška planina landslide (NW Slovenia) using UAV photogrammetry and tachymetric measurements. *Landslides*, 14, 395–406. <https://doi.org/10.1007/s10346-016-0759-6>
- Pijl, A., Bailly, J. S., Feurer, D., El Maaoui, M. A., Boussemma, M. R., & Tarolli, P. (2020). TERRA: Terrain extraction from elevation rasters through repetitive anisotropic filtering. *International Journal of Applied Earth Observation and Geoinformation*, 84, 101977. <https://doi.org/10.1016/j.jag.2019.101977>
- Pirotti, F., & Tarolli, P. (2010). Suitability of LiDAR Point Density and Derived Landform Curvature Maps for Channel Network Extraction. *Hydrological Processes*, 24, 1187–1197. <https://doi.org/10.1002/hyp.7582>
- Podolszki, L., Kurečić, T., Bateson, L., & Svennevig, K. (2022). Remote Landslide Mapping, Field Validation and Model Development – An Example from Kravarsko, Croatia. *Geologia Croatica*, 75(1), 67–82. <https://doi.org/10.4154/gc.2022.01>
- Prokešová, R., Kardoš, M., & Medveďová, A. (2010). Landslide dynamics from high-resolution aerial photographs: A case study from the Western Carpathians, Slovakia. *Geomorphology*, 115(1–2), 90–101. <https://doi.org/10.1016/j.geomorph.2009.09.033>
- QGIS Python Plugins Repository (2019). Plugins by Kosuke ASAHI. <https://plugins.qgis.org/plugins/author/Kosuke%20ASAH/>
- QGIS Python Plugins Repository (2021). Virtual Raster Builder. <https://plugins.qgis.org/plugins/vrtbuilderplugin/>
- QGIS Python Plugins Repository (2022). Qgis2threejs. <https://plugins.qgis.org/plugins/Qgis2threejs/>
- QGIS Python Plugins Repository (2023). qProf 0.5.1. <https://plugins.qgis.org/plugins/qProf/version/0.5.1/>
- Razak, K. A., Straatsma, M. W., van Westen, C. J., Malet, J.-P., & de Jong, S. M. (2011). Airborne laser scanning of forested landslides characterization: Terrain model quality and visualization. *Geomorphology*, 126, 186–200. <https://doi.org/10.1016/j.geomorph.2010.11.003>
- Roberts, A. (2001) Curvature attributes and their application to 3D interpreted horizons. *First Break*, 19, 85–99. <https://onlinelibrary.wiley.com/doi/abs/10.1046/j.0263-5046.2001.00142.x>
- Rossi, G., Tanteri, L., Tofani, V., Vannocci, P., Moretti, S., & Casagli, N. (2018). Multitemporal UAV surveys for landslide mapping and characterization. *Landslides*, 15, 1045–1052. <https://doi.org/10.1007/s10346-018-0978-0>
- SAGA-GIS Module Library Documentation (v2.2.0). Module Sky View Factor (2008). http://www.saga-gis.org/saga_tool_doc/2.2.0/ta_lighting_3.html
- SAGA-GIS Tool Library Documentation (v2.2.0) (2005). Module Supervised Classification for Grids. https://saga-gis.sourceforge.io/saga_tool_doc/2.2.0/imagery_classification_0.html
- SAGA-GIS Tool Library Documentation (v2.2.1). Module Slope, Aspect, Curvature (2001). https://saga-gis.sourceforge.io/saga_tool_doc/2.2.1/ta_morphometry_0.html
- SAGA-GIS Module Library Documentation (v2.2.1). Module Wombling (Edge Detection) (2015). https://saga-gis.sourceforge.io/saga_tool_doc/2.2.1/grid_filter_16.html
- Satari, B., & Kazimi, M. (2021). Extraction of linear structures from digital terrain models using deep learning. *AGILE GIScience Series*, 2(11), 1–14. <https://doi.org/10.5194/agile-giss-2-11-2021>
- Schillaci, C., Braun, A., & Kropáček, J. (2015). Terrain analysis and landform recognition. In L. Clarke, & J. Nield, (Eds.), *Geomorphological Techniques* (pp. 1–18). British Society for Geomorphology.
- Shary, P. A., Sharaya, L. S., & Mitusov, A. V. (2002). Fundamental Quantitative Methods of Land Surface Analysis. *Geoderma*, 107, 1–32. [http://dx.doi.org/10.1016/S0016-7061\(01\)00136-7](http://dx.doi.org/10.1016/S0016-7061(01)00136-7)
- Shruthi, R. B., Kerle, N., & Jetten, V. (2011). Object-based gully feature extraction using high spatial resolution imagery. *Geomorphology*, 134(3–4), 260–268. <https://doi.org/10.1016/j.geomorph.2011.07.003>
- Šimeková, J., Martinčeková, T., Abrahám, P., Gejdoš, T., Grenčíková, A., Grman, D., ..., & Sluka V. (2006). The Atlas of the slope stability maps of the Slovak Republic at a scale 1:50,000. MŽP SR. <https://ags.geology.sk/arcgis/services/WebServices/SD/MapServer/WMServer>
- Slámová, M., Pažinová, N. B., Belčáková, I., Beljak, J., & Maliniak, P. (2023). Identification of historical trackways in forests using contextual geospatial analyses. *Archaeological Prospection*, 30(2), 135–152. <https://doi.org/10.1002/arp.1882>
- Sofia, G., Tarolli, P., Cazorzi, F., & Dalla Fontana, G. (2010). Channel Network Identification from High-Resolution DTM: A Statistical Approach. *Hydrology and Earth System Sciences*, 7, 9327–9365.
- Strydom, T., & Poisot, T. (2023). SpatialBoundaries.jl: edge detection using spatial wombling. *Ecography*, 5, e06609. <https://doi.org/10.1111/ecog.06609>
- Štular, B., Kopalj, Ž., Oštir, K., & Nuninger L. (2012). Visualisation of lidar-derived relief models for detection of archaeological features. *Journal of Archaeological Science*, 39(11), 3354–3360. <https://halshs.archives-ouvertes.fr/halshs-00743691>
- Syzdykbayev, M., Karimi, B., & Karimi, H. A. A. (2020). Method for extracting some key terrain features from shaded relief of digital terrain models. *Remote Sensing*, 12, 2809.
- Tarolli, P., Pijl, A., Cucchiaro, S., & Wei, W. (2020). Slope instabilities in steep cultivation systems: Process classification and opportunities from remote sensing. *Land Degradation & Development*, 32, 1368–138. <https://doi.org/10.1002/ldr.3798>
- The Geodesy, Cartography and Cadastre Authority of the Slovak Republic (2023a). Geoportal Download. Digital Terrain Model DMR3.5. https://opendata.skgeodesy.sk/static/DMR3_5/dmr3_5-10.zip
- The Geodesy, Cartography and Cadastre Authority of the Slovak Republic (2023b). ZBGIS®. Map Client Terrain. <https://zbgis.skgeodesy.sk/mkzbgis/sk/teren/toc/dmr5/>
- The Geodesy, Cartography and Cadastre Authority of the Slovak Republic (2023c). Aerial Laser Scanning and DMR 5.0. <https://www.geoportal.sk/files/zbgis/lis/parametre-lokality-zberu-udajov-lis.pdf>
- The Geodesy, Cartography and Cadastre Authority of the Slovak Republic (2023d). Orthomosaic 2023. https://zbgisws.skgeodesy.sk/zbgis_ortofoto_wms/service.svc/get
- Thomas, I. A., Jordan, P., Shine, O., Fenton, O., Mellander, P. E., Dunlop, P., & Murphy, P. N. C. (2017). Defining optimal DEM resolutions and point densities for modelling hydrologically sensitive areas in agricultural catchments dominated by microtopography. *International Journal of Applied Earth Observation and Geoinformation*, 54, 38–52. <https://doi.org/10.1016/j.jag.2016.08.012>
- Turner, D., Lucieer, A., & De Jong, S. M. (2015). Time Series Analysis of Landslide Dynamics Using an Unmanned Aerial Vehicle (UAV). *Remote Sensing*, 7, 1736–1757. <https://doi.org/10.3390/rs70201736>

- Tzvetkov, J. (2018). Relief visualization techniques using free and open source GIS tools. *Polish Cartographical Review*, 50, 61–71. <https://doi.org/10.2478/pcr-2018-0004>
- Van Den Eeckhaut, M., Poesen, J., Verstraeten, G., Vanacker, V., Moeyersons, J., Nyssen, J., & Van Beek, L. (2005). The effectiveness of hillshade maps and expert knowledge in mapping old deep-seated landslides. *Geomorphology*, 67(3–4), 351–363. <https://doi.org/10.1016/j.geomorph.2004.11.001>
- Van Den Eeckhaut, M., Poesen, J., Verstraeten, G., van Acker, V., Nyssen, J., Moeyersons, J., ..., & Vandekerckhove, L. (2007). The use of LIDAR-derived images for mapping old landslides under forest. *Earth Surface Process*, 32, 754–769.
- Wilson, J. P. (2012). Digital terrain modeling. *Geomorphology*, 137(1), 107–121. <https://doi.org/10.1016/j.geomorph.2011.03.012>
- Yan, G., Tang, G., Chen, J., Li, F., Yang, X., Xiong, L., & Lu, D. (2024). Modeling computer sight based on DEM data to detect terrain breaks caused by gully erosion on the loess Plateau. *Catena*, 237, 107837.
- Zêzere, J. L. (2002). Landslide susceptibility assessment considering landslide typology. A case study in the area north of Lisbon (Portugal). *Natural Hazards and Earth System Sciences*, 2(1/2), 73–82. <https://doi.org/10.1007/s12517-017-2980-6>
- Zhao, H., Fang, X., Ding, H., Josef, S., Xiong, L., Na, J., & Tang, G. (2017). Extraction of terraces on the Loess Plateau from high-resolution DEMs and imagery utilizing object-based image analysis. *ISPRS International Journal of Geo-Information*, 6(6), 157. <https://doi.org/10.3390/ijgi6060157>
- Zhou, X., Li, W., & Arundel, S. T. (2018). A spatio-contextual probabilistic model for extracting linear features in hilly terrains from high-resolution DEM data. *International Journal of Geographical Information Science*, 33, 666–686. <https://doi.org/10.1080/13658816.2018.1554814>

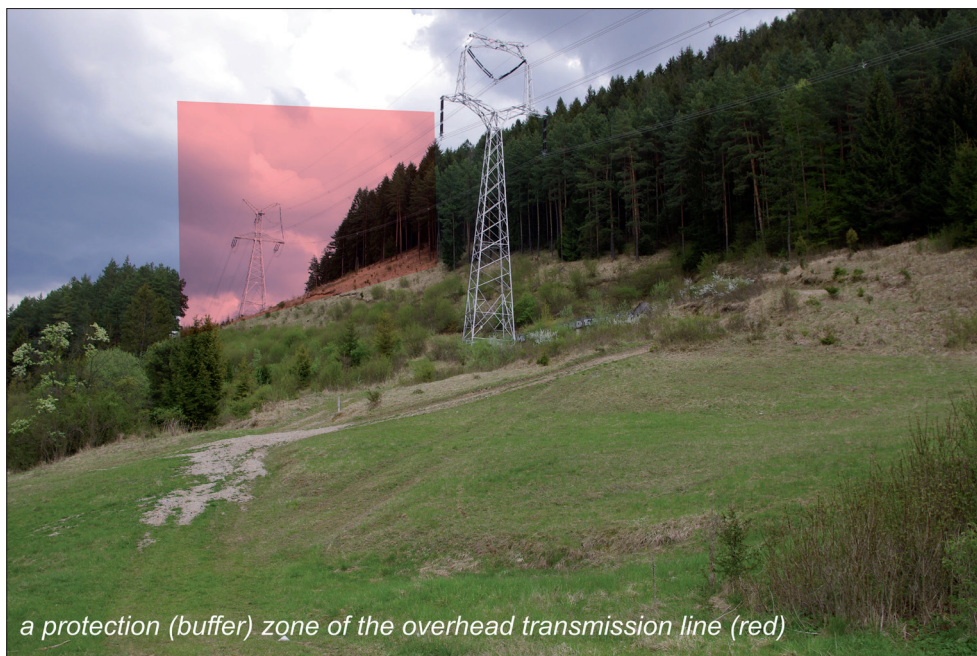
Please cite this article as:

Slámová, M., Sitko, R., Kadlečík, R., Skurčák, E., & Chudý, F. (2025). Detection and visualisation of terrain edges in slope failures. *Moravian Geographical Reports*, 33(2), 70–90. <https://doi.org/10.2478/mgr-2025-0006>

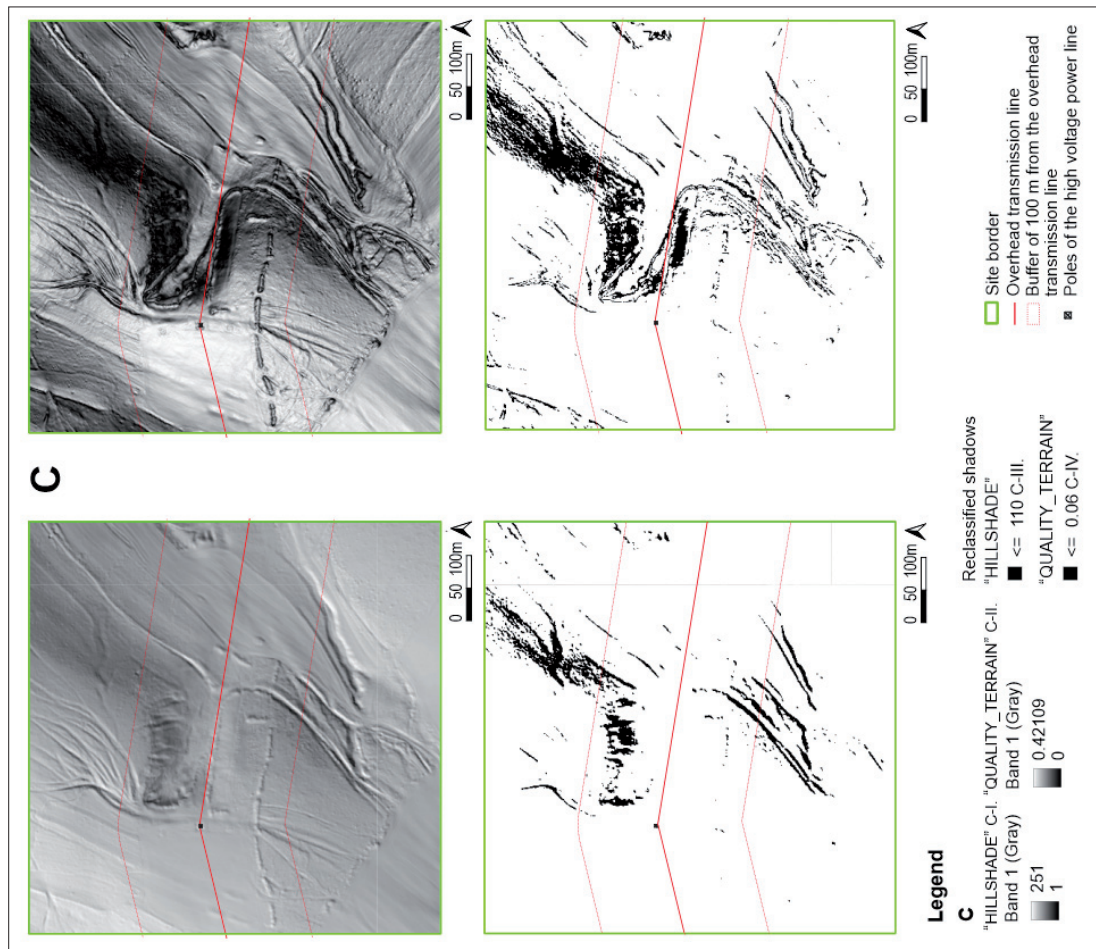
Appendices

Appendix 1: The protection buffer zone (100 m) of the overhead transmission powerline

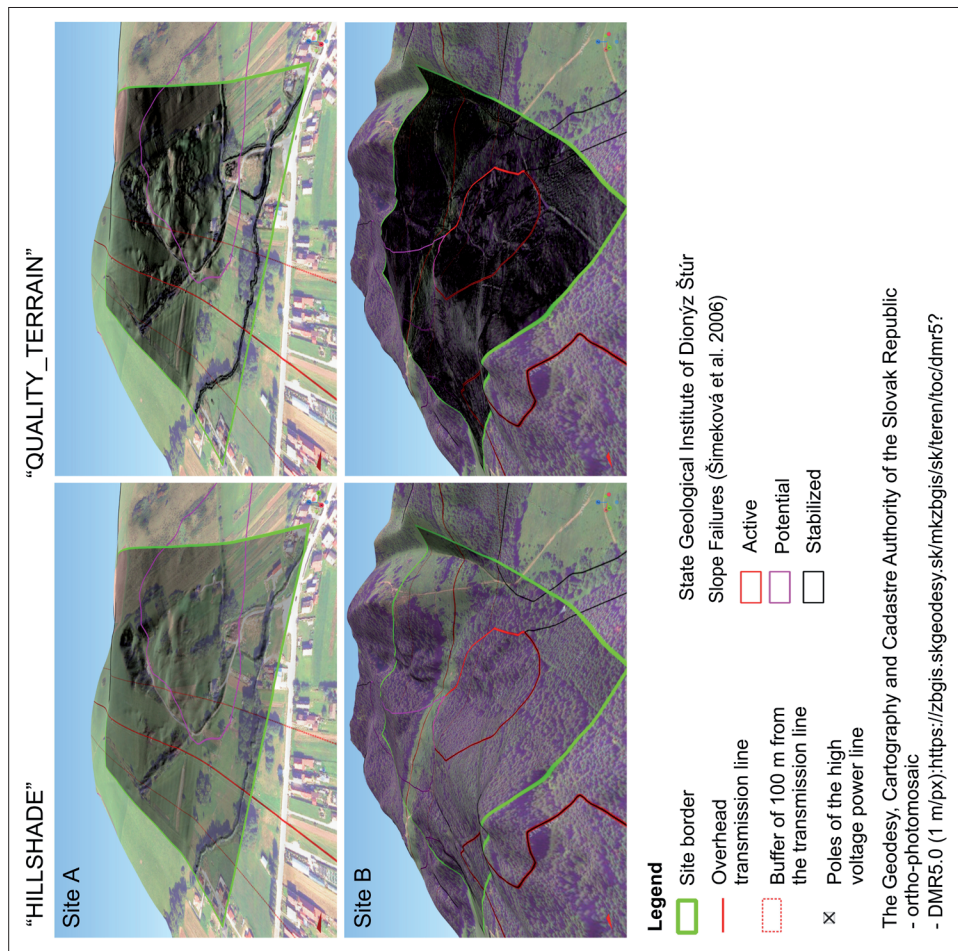
Photos: M. Slámová (2023)



Appendix 2: Visual comparison between C-I. – the grayscale grid of "HILLSHADE" and C-II. – "QUALITY_TERRAIN", visual comparison between C-III. – reclassified grayscale grid to binary grid of "QUALITY_TERRAIN" of "HILLSHADE" and C-IV. – reclassified grayscale grid to binary grid of "QUALITY_TERRAIN"
 Source: VUJE a.s.: overhead transmission powerline, poles and protection zone, The Geodesy, Cartography and Cadastre Authority of the Slovak Republic: DMR5.0 (1 m) JTTSK(JTTSK03), Cartography and Cadastre Authority of the Slovak Republic: DMR5.0 (1 m) JTTSK(JTTSK03), modified by the author

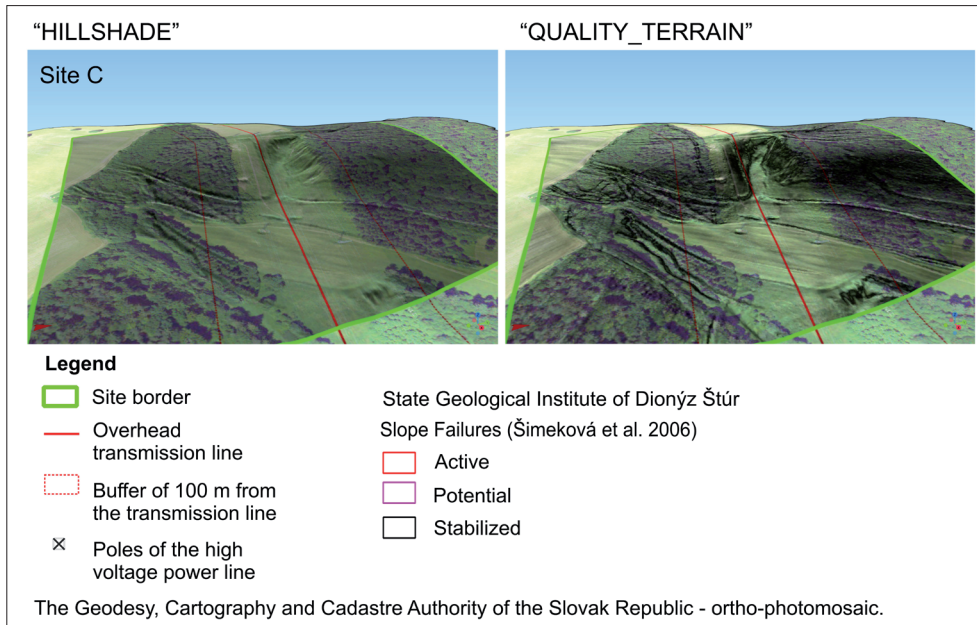


Appendix 3: Sites A, B – Spatial visualisations created from DMR5.0 with "HILLSHADE" and "QUALITY_TERRAIN" overlapped with ortho-photomosaic
 Source: VUJE a.s.: overhead transmission powerline, poles and protection zone, The Geodesy, Cartography and Cadastre Authority of the Slovak Republic: DMR5.0 (1 m) JTTSK(JTTSK03) and ortho-photomosaic, State Geological Institute of Dionýz Štúr: slope failures, modified by the author



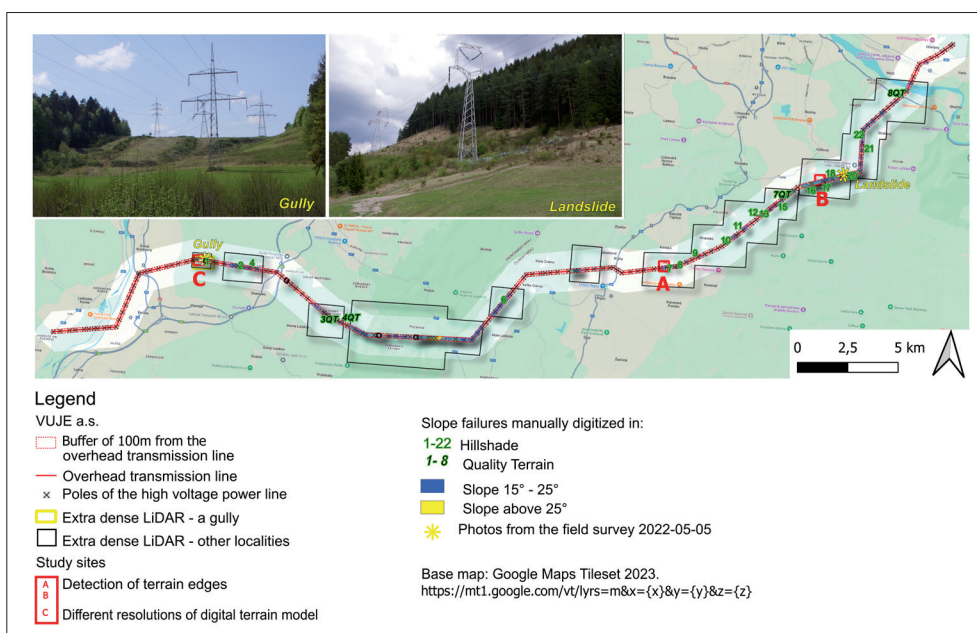
Appendix 4: Site C – Spatial visualisations created from DMR5.0 with “HILLSHADE” and “QUALITY_TERRAIN” overlapped with ortho-photomosaic

Source: VUJE a.s.: overhead transmission powerline, poles and protection zone, The Geodesy, Cartography and Cadastre Authority of the Slovak Republic: DMR5.0 (1 m) JTSK(JTSK03) and ortho-photomosaic, State Geological Institute of Dionýz Štúr: slope failures, modified by the author

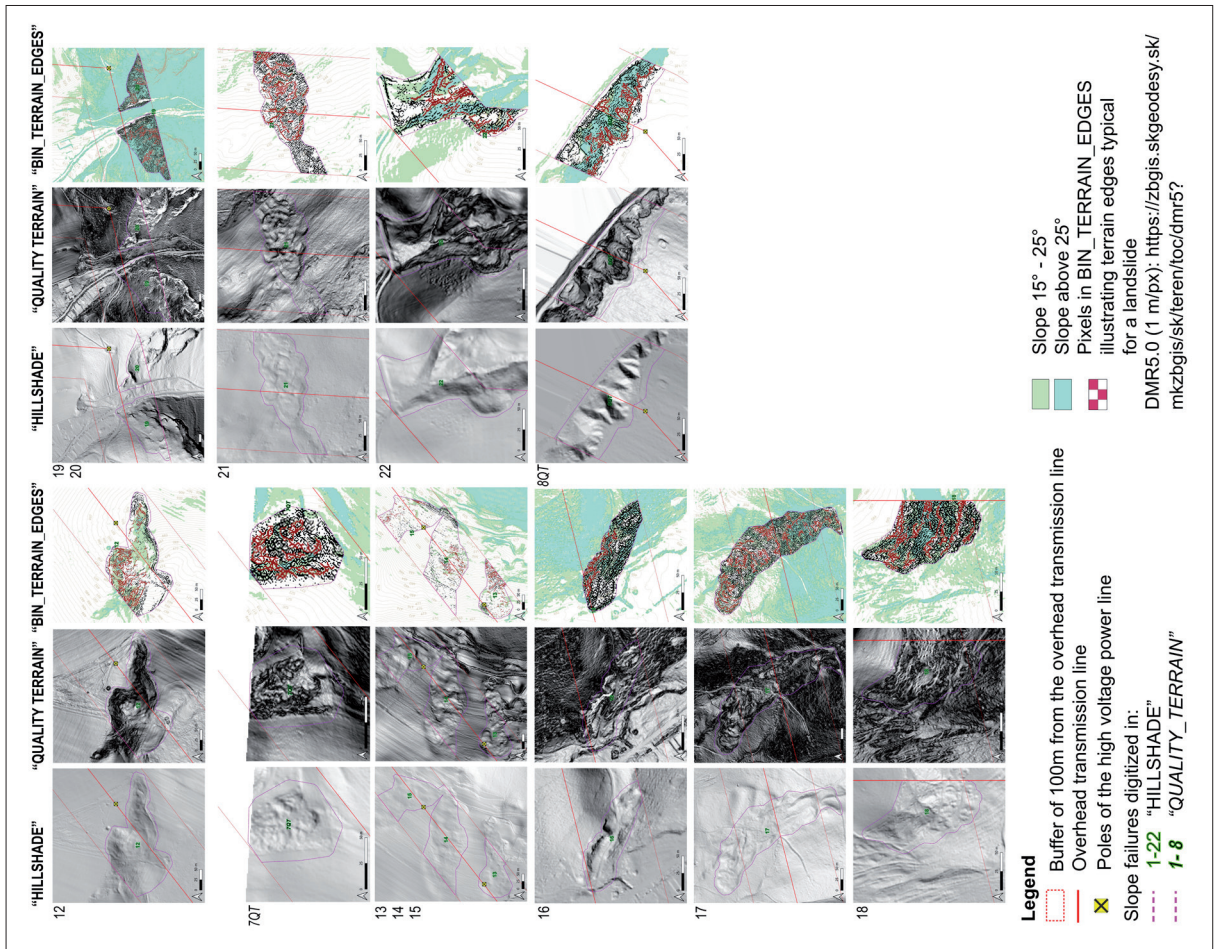
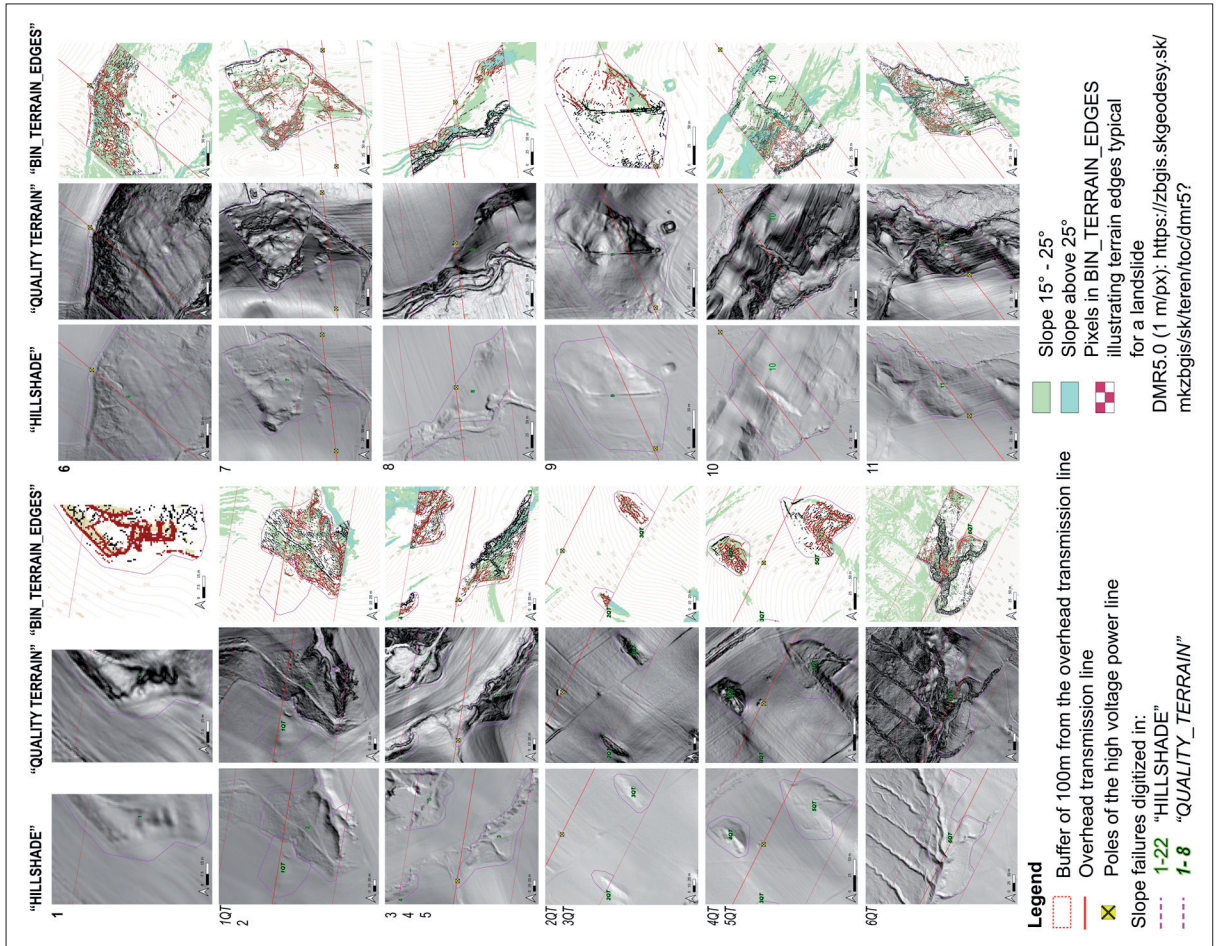


Appendix 5: Slope failures digitised on the basis of “HILLSHADE” and “QUALITY_TERRAIN” and their location on slopes of different categories

Source: VUJE a.s.: overhead transmission powerline, poles and protection zone, Google Maps Tileset, modified by the author; author’s elaboration: “HILLSHADE”, “QUALITY_TERRAIN” and slope; photos: M. Slámová (2023)



Appendices 6-1 (left) and 6-2 (right): Interpretation of digitised slope failures in "HILLSHADE", "QUALITY_TERRAIN" and "BIN_TERRAIN_EDGES" on different slopes. Red coloured is a pattern of slope matching shapes of scarps, cracks and transversal ridges (defined in methodology)
 Source: VUJE a.s.: overhead transmission powerline, poles and protection zone, The Geodesy, Cartography and Cadastre Authority of the Slovak Republic: DMR5.0 (1 m) JTSK(JTSK03), modified by the author; author's elaboration: "HILLSHADE", "QUALITY_TERRAIN" and slope



Appendix 7: Site C: Application of the new method to different resolutions of digital terrain models to identify terrain edges on slopes in "QUALITY_TERRAIN"

Source: VUJE a.s.: overhead transmission powerline, poles, protection zone and extra dense LiDAR, The Geodesy, Cartography and Cadastre Authority of the Slovak Republic: DMR5.0 (1 m) JTSK(JTSK03) and DMR3.5 modified by the author; author's elaboration: "HILLSHADE", "QUALITY_TERRAIN"; photo: M. Slámová (2023)

